Cell splitting in *Staphylococcus aureus* is controlled by an adaptor protein facilitating degradation of a peptidoglycan hydrolase

Maria Disen Barbuti[1¶], Eivind Frøyland Skjennum[1¶], Viktor Hundtofte Mebus[2], Danae Morales Angeles[1], Matilde Hustad[1], Marita Torrissen Mårli[1], Dorte Frees[2], and Morten Kjos[1*]

[1]Faculty of Chemistry, Biotechnology and Food Science, Norwegian University of Life Sciences, Ås, Norway

[2]Department of Veterinary and Animal Sciences, Faculty of Health and Medical Sciences, University of Copenhagen, Copenhagen, Denmark

*Corresponding author

Email: morten.kjos@nmbu.no

¶These authors contributed equally to this work

Abstract

Regulated protein degradation by Clp proteases is a highly conserved post-translational control mechanism in bacteria. In *Staphylococcus aureus*, the ClpXP complex targets the peptidoglycan hydrolase Sle1, maintaining a tightly regulated balance between peptidoglycan biosynthesis and hydrolysis, which is required to ensure proper cell splitting without compromising cell integrity. β-lactams antibiotics disturb this balance, leading to their bactericidal effects. The mechanism underlying the specific targeting of Sle1 by the conserved ClpXP complex remains unknown. From a genome-wide screen for determinants of penicillin G susceptibility in *S. aureus*, we here identify the uncharacterized protein CxaR (for ClpXP-associated autolytic regulator). Growth defects, premature cell splitting, and increased cell lysis were observed in the absence of CxaR. Interestingly, these defects were mitigated by sublethal concentrations of β-lactams. Through sequencing *cxaR* suppressor mutants, followed by immunoblotting, we show that the *cxaR* phenotypes are caused by excessive Sle1 accumulation. Indeed, exposure to β-lactams reduces Sle1 levels, thereby rescuing the cells lacking CxaR. Furthermore, *in vivo* protein-protein interaction assays demonstrated that CxaR directly interacts with both ClpXP and Sle1, whereas no direct interaction was detected between Sle1 and ClpX. In line with this, CxaR was found to co-localize with ClpX adjacent to the septum. Taken together, these findings reveal that CxaR is a new regulatory factor controlling staphylococcal cell splitting by acting as an adaptor protein for controlled ClpXP-mediated degradation of Sle1.

Introduction

Bacterial proliferation depends on the precise coordination of cell division, a complex process that culminates in the separation of daughter cells. In the Gram-positive coccoid pathogen *Staphylococcus aureus*, division initiates with the synthesis of a septal cross-wall at midcell, generating two hemispherical daughter cells that remain transiently connected via a peripheral wall ring [1-4]. Only after the septum is fully formed does this septum-adjacent peripheral cell wall undergo rapid resolution ("popping") [1, 2]. This step, occurring in less than two milliseconds, is highly regulated to prevent premature splitting of the septum, which would compromise cell integrity and viability, ultimately leading to cell lysis [5, 6]. Septal splitting is facilitated by peptidoglycan hydrolases (PGHs) that create small perforations in the peripheral peptidoglycan ring, causing mechanical crack propagation [1, 7]. *S. aureus* encodes at least 20 PGHs with different physiological roles during bacterial growth and division [5, 8]. Among these, the amidase Sle1, which cleaves the amide bond linking the stem peptide to the glycan chain, plays a particularly important role in cell splitting, as its absence results in cell clustering, delays in cell cycle progression, and the formation of tetrad cells [2, 7, 9, 10]. Sle1 is translocated to the extracellular milieu by active secretion, facilitated by its N-terminal signal peptide. Three cell wall-binding LysM domains ensure localization to the division septum, where the catalytic CHAP domain facilitates peptidoglycan cleavage [11, 12].

As with all PGHs, Sle1 activity must be tightly regulated both spatially and temporally to prevent unintended breaches in the cell wall [5, 6]. Targeted recruitment of these enzymes to specific regions of the cell serves as a key regulatory mechanism in many bacteria, including *S. aureus* [11, 13, 14]. The localization of Sle1 is dependent on the anionic glycopolymers wall teichoic acids (WTAs). The reduced levels of WTA at the septum promote Sle1 accumulation and peptidoglycan cleavage in this region [11, 15]. The two-component systems WalKR and GraSR, facilitates transcriptional regulation of Sle1, ensuring proper coordination of cell wall remodeling and division [16-19]. Furthermore, recent studies have identified the DNA

68 translocase and cell division protein FtsK [10] as well as a non-coding RNA named Rbc1 [20]
69 as positive regulators of Sle1. Finally, and importantly, Sle1 levels are regulated by the ClpXP
70 protease through targeted degradation [7].
71
72 Regulated protein degradation by Clp proteases affects all biological pathways, playing a
73 crucial role in both general protein quality control and the targeted degradation of specific
74 proteins in bacterial cells [21-23]. The ClpXP complex consist of the ATP-dependent hexameric
75 ClpX ring, which recognizes, unfolds, and translocates specific protein substrates into the ClpP
76 proteolytic chamber for degradation [24]. While ClpXP can directly target various substrates,
77 efficient recognition of certain proteins requires separately encoded adaptor proteins that
78 recognize specific substrates and assist in their delivery to ClpXP for degradation [21-23]. The
79 vital roles of ClpXP adaptor proteins have been characterized in different bacteria, including
80 *Escherichia coli* with SspB [25-27], UmuD [28, 29], and RssB [30, 31]. The only known adaptor
81 protein for ClpXP in *S. aureus* is YjbH, which targets the stress-associated transcriptional
82 regulator Spx for degradation [32-34], similar to its role in *B. subtilis* [35, 36].
83
84 Only a few ClpXP substrates have been verified in *S. aureus*, including Spx and Sle1 [37-39].
85 Unlike Spx, the mechanism by which ClpXP recognizes Sle1 is unknown. Nonetheless, the
86 targeted degradation of Sle1 has been shown to be crucial for the survival of staphylococcal
87 cells [7, 39-41]. Deletion of *clpX* results in abnormal septum formation and premature splitting
88 of daughter cells [40-42]. This phenotype is mainly attributed to the impaired proteolytic
89 regulation and subsequent accumulation of PGHs, particularly Sle1 [7, 38-40, 42, 43]. Beyond
90 proteolysis, ClpX also appears to contribute to cell division independently of ClpP, as only *clpX*
91 mutants exhibit heat stability and cold sensitivity [39, 44], a temperature dependent growth
92 defect that can be alleviated by a mutation in the essential cell division protein FtsA [43]. ClpX
93 has additionally been found to impact transcription of genes involved in peptidoglycan
94 synthesis and cell division independently of ClpP [45]. Interestingly, addition of β-lactams,
95 inhibition of lipoteichoic acid (LTA) and wall teichoic acid (WTA) biosynthesis, or inactivation of

96 Sle1 can rescue growth of *clpX* mutants [41, 42], further evidencing a tight interplay between
97 ClpXP, Sle1 and cell wall biogenesis in *S. aureus*.
98
99 The wide range of regulatory mechanisms invested into governing PGHs, and particularly Sle1,
100 underlines the importance of maintaining control of these enzymes. Indeed, the bactericidal
101 mechanism of β-lactam antibiotics appears to involve the dysregulation of PGH activity [46].
102 β-lactams inhibit the peptidoglycan cross-linking capacity of penicillin-binding proteins (PBPs)
103 by covalently binding their active site [47-49]. This is believed to disturb the delicate balance
104 between polymerization and autolytic degradation of peptidoglycan, which ultimately result in
105 cell lysis [46, 50-52]. The relationship between PBPs and PGHs appears to be highly complex.
106 On one hand, low-dose treatment with β-lactams result in thickened septal walls, delay cell
107 separation, and significantly reduce the levels of specific PGHs, including Sle1 [7, 41, 53-56].
108 These findings suggest that β-lactams may exert their bactericidal effects, in part, by lowering
109 the activity of specific PGHs, resulting in aberrant septum formation that does not permit further
110 cell growth and division. [49, 50, 57]. On the other hand, β-lactam treatment has frequently
111 been associated with activation of PGHs, leading to excessive cell wall degradation and
112 subsequent cell lysis [50-52, 57]. Studies in various bacteria, including *Streptococcus*
113 *pneumoniae* and *Bacillus subtilis*, have shown that when autolytic activity is suppressed,
114 exposure to penicillin primarily results in growth inhibition rather than lysis [49, 50, 57]. The
115 contrasting observations underscore that the exact mode of action of β-lactams is more
116 complex than initially assumed and may depend on species-specific factors.
117
118 In the current study, we show that SAOUHSC_00659, a hitherto uncharacterized protein here
119 renamed CxaR (for ClpXP-associated autolytic regulator), controls cellular levels of Sle1 by
120 mediating its targeted degradation by the ClpXP complex. Deletion or knockdown of the gene
121 encoding CxaR resulted in accumulation of Sle1, which in turn contributed to growth
122 deficiencies, accelerated daughter cell splitting, and increased cell lysis. Co-localization
123 analyses combined with protein-protein interaction assays revealed that CxaR depends on

124 ClpX for its septal-adjacent localization. While both proteins directly interact with each other,
125 our results suggest that only CxaR interacts with Sle1. Together, these findings identify and
126 elucidate the mechanism of a new adaptor protein required for spatiotemporal regulation of
127 bacterial cell splitting.

128 # Results

129 **Sublethal concentrations of cell wall targeting antibiotics stimulate growth of cells**
130 **lacking *cxaR***

131 A genome-wide, pooled CRISPR interference sequencing (CRISPRi-seq) screen [58-60] was
132 conducted to identify genetic factors modulating susceptibility to β-lactams in *S. aureus*
133 NCTC8325-4 (see **S1 Table** and **S1 Fig**). By knocking down the expression of transcriptional
134 units, both in the presence and absence of inhibitory concentrations of penicillin G, we could
135 quantify the associated growth fitness cost for each unit. The most prominent hit from this
136 screen was a gene of unknown function, *SAOUHSC_00659* (hereafter referred to as *cxaR*),
137 whose knockdown led to reduced fitness, an effect that appeared to be counteracted by the
138 presence of penicillin G (**S1 Fig**).

139

140 To validate this result, a *cxaR* CRISPRi knockdown strain was created in *S. aureus* NCTC8325-
141 4. CxaR depletion resulted in a distinct growth profile in TSB at 37°C, characterized by reduced
142 initial growth rate, followed by a transient decline in optical density (OD), and a subsequent
143 gradual recovery of growth (**Fig 1A)**. The growth defect of *cxaR* knockdown was similar,
144 although even more pronounced, in the MRSA strain JE2 (**Fig 1A**). A *cxaR* deletion mutant
145 was also constructed in NCTC8325-4 by allelic exchange with a spectinomycin resistance
146 cassette. The resulting strain (NCTC8325-4 Δ*cxaR*::*spc*) exhibited the same biphasic growth
147 (**Fig 1B**), confirming that the growth phenotype was not caused by the CRISPRi-system.
148 Finally, to exclude the possibility that the phenotype observed upon knockdown or deletion of
149 *cxaR* was caused by polar effect on neighboring genes, we designed sgRNAs for CRISPRi
150 knockdown of five adjacent genetic loci, located both upstream and downstream of *cxaR* (**S2A**
151 **Fig**). Growth analyses revealed that none of these strains exhibited growth patterns similar to
152 the *cxaR* mutant (**S2B-C Fig**), confirming that the observed effects are specifically attributable
153 to *cxaR*.

154

155 Strikingly, and in line with the results from the CRISPRi-seq screen, subinhibitory
156 concentrations of penicillin G rescued the growth defects of the *cxaR* knockdown and deletion
157 mutants. When treated with penicillin G, the mutants grew similarly to the controls, both in
158 liquid and on solid medium (**Fig 1**, **S3A Fig**, **S5A Fig**). The minimal inhibitory concentration
159 (MIC) of the *cxaR* mutants, however, remained unaltered (**S3A Fig**).
160
161 To determine whether the penicillin G-mediated growth stimulation was a general response to
162 growth inhibition or specific to certain antibiotics, the JE2 *cxaR* knockdown strain was tested
163 against a panel of antibiotics, targeting different cellular processes (**Fig 1D** and **S3 Fig**).
164 Subinhibitory concentrations of all tested β-lactams (penicillin G, oxacillin, and cefoxitin) fully
165 rescued growth of CxaR depleted cells (**Fig 1D**, **S3A-C Fig**). Similarly, other antibiotics
166 targeting the cell wall, such as moenomycin (inhibiting transglycosylation activity) and
167 tunicamycin (inhibiting early stages in wall teichoic acid and peptidoglycan biosynthesis), also
168 fully restored growth (**Fig 1D**, **S3G-H Fig**). Partial growth rescue was observed for bacitracin
169 (inhibiting lipid carrier recycling) and teicoplanin (glycopeptide inhibiting cell wall synthesis by
170 binding to the D-Ala-D-Ala terminus of peptidoglycan precursors), while another glycopeptide
171 with the same mechanism of action, vancomycin, did not seem to stimulate growth (**Fig 1D**,
172 **Fig S3D-F**). Furthermore, translation inhibitors binding to the 30S ribosomal subunit, including
173 kanamycin and streptomycin, as well as the DNA gyrase inhibitor novobiocin, partially restored
174 growth of the CxaR depleted strain (**Fig 1D**, **S3N,O,J Fig**). On the other hand, the tested
175 antibiotics targeting topoisomerase IV (ciprofloxacin), folate biosynthesis (trimethoprim),
176 transcription (rifampicin), and the 50S ribosomal subunit (erythromycin) did not stimulate
177 growth at any concentration (**Fig 1D**, **S3I,K,L,M Fig**).
178

179 **CxaR is conserved among *Staphylococcaceae* and has structural resemblance to TPR**
180 **motifs**

181 *cxaR* is part of the *S. aureus* core genome, and phylogenetic analysis of CxaR homologues
182 from 55 different species within the *Staphylococcaceae* family demonstrated a high degree of
183 conservation among the homologs from the closely related genera *Staphylococcus*,
184 *Macrococcus*, and *Mammaliicoccus*, with 44 out of 165 amino acids being completely
185 invariable (**S4A-B Fig**). *cxaR* does not encode any signal peptide nor any transmembrane
186 helices. The high-confidence AlphaFold-predicted structure of CxaR consists of two short N-
187 terminal α-helices, six similarly sized antiparallel α-helices forming a slightly concave groove,
188 and finally a longer C-terminal α-helix protruding from the rest of the structure (**Fig 1E)**. When
189 mapping residue conservation onto the predicted structure of CxaR, we found that highly
190 conserved residues were primarily located at positions mediating hydrophobic interactions
191 between the antiparallel α-helices and within the groove (**Fig 1E**, **S4 Fig**). HHpred [61] and
192 HMMER [62] were used to identify potential protein domains of CxaR. Interestingly, both tools
193 revealed a substantial number of significant hits with tetratricopeptide repeat (TPR) motifs.
194 TPR motifs consist of 34-residue antiparallel helix pairs, typically repeated 3 to 16 times to
195 form grooved, amphipathic binding surfaces that facilitate protein-protein interactions [63].
196 Although the sequences of TPR motifs are highly variable and therefore at times difficult to
197 detect, they are involved in a wide range of cellular processes [64, 65]. The most probable
198 TPR helix pairs of CxaR, along with the resulting binding groove, are labelled in **Fig 1E**.
199

200 **CxaR affects splitting of daughter cells**

201 To better understand the growth phenotypes of the *cxaR* mutants, phase contrast and
202 epifluorescence microscopy were performed on samples taken at different stages of growth
203 (indicated in **Fig 2A**). Cells lacking CxaR clearly displayed increased lytic activity. Even before
204 the drop in OD, a noticeably higher proportion of mutant cells appeared lysed compared to
205 wild-type cells (hour 6 and 8, **Fig 2B and D**, **S5 Fig**). While the morphology of the live mutant
206 cells did not significantly diverge from the wild-type, including comparable cell size (**Fig 2C**),
207 we often observed *cxaR* mutant cells with a nick at septum displaying DNA dispersal, as
208 visualized by DAPI-staining (**Fig 2B and D**). After the temporal decline in OD, few intact cells

209 remained, and a large amount of cellular debris was observed (**Fig 2B**). During the subsequent
210 growth recovery phase, less lysis was observed. Strikingly, addition of penicillin G to cells
211 lacking CxaR significantly reduced lysis at all recorded time points, with a particularly notable
212 reduction at the 10-hour mark, when the majority of CxaR-deficient cells would otherwise have
213 lysed (**S5 Fig**).
214
215 CxaR overexpression was also analyzed (**Fig 2E-F**). Elevated levels of CxaR did not result in
216 any growth deficiency. In fact, these cells reach a slightly higher final OD compared to those
217 with normal CxaR levels (**Fig 2F**). Morphologically, cells with excess CxaR clustered together,
218 frequently forming tetrads, where a second round of division is initiated before the previous
219 pair of daughter cells have separated (**Fig 2E**). Notably, very few of the CxaR overexpressing
220 cells were observed without a septum, indicating that excess CxaR does not impair septum
221 synthesis but rather disrupts the separation of daughter cells after septum completion.
222
223 The lysis phenotype was further investigated by transmission electron microscopy (TEM). As
224 expected, TEM analysis of CxaR depleted cells also revealed a significantly higher proportion
225 of lysed cells compared the control strain (**Fig 3A and C**). Consistent with earlier observations,
226 penicillin-treated *cxaR* samples showed a drastic reduction in lysis compared to the untreated
227 samples (**Fig 3A and C**). Interestingly, the mutant cells frequently displayed premature splitting
228 of daughter cells, where the septum appeared to be degraded before it was completed (marked
229 with red asterisks in **Fig 3A and G-I**). Variations of this phenotype were observed, with some
230 cells exhibiting a nick prior to or at early stages of septal growth (**Fig 3G**), while others
231 underwent splitting just before septum completion (**Fig 3H**). Some cells also underwent
232 splitting at both ends of the septum simultaneously (**Fig 3I**). Furthermore, while most live *cxaR*
233 cells resembled the control cells (**Fig 3D-E**), a subset exhibited a significantly thicker cell wall
234 (**Fig 3F**), potentially a strategy adapted by some mutant cells to evade lysis. Taken together,
235 these findings indicate that the lysis observed in cells lacking CxaR is due to premature septum
236 splitting, and that penicillin G mitigates this by preventing spontaneous lysis in the mutant.

237

238 **Reduced Sle1 activity can compensate for the lack of CxaR**

239 Since cell splitting in *S. aureus* is known to be temperature-responsive [20], we examined the
240 growth of *cxaR* mutant cells across a range of temperatures. The mutants exhibited a clear
241 temperature-dependent growth phenotype (**Fig 4A**, **S6 Fig**); the growth defect was
242 exaggerated at 30°C, while it was recovered at higher temperatures (42-45°C). Notably, when
243 plated at 30°C, the *cxaR* deletion mutant displayed heterogeneous colony size, with both small
244 and large-sized colonies, in contrast to the uniform, large colony size of the wild-type (**Fig 4B**).
245 The colony size variation also appeared at 37°C, although to a lesser extent (**Fig 4A**, **S6B**
246 **Fig**). We hypothesized that the larger sized colonies at 30°C had obtained suppressor
247 mutations. Five Δ*cxaR* colonies were picked and shown to exhibit wild-type like growth patterns
248 (**Fig 4B and 4C**). Whole-genome re-sequencing of these mutants revealed that each had
249 independently acquired additional mutations associated with the PGH *sle1* (**S2 Table**). Two of
250 the suppressor mutants had substitutions in the catalytically active CHAP-domain, responsible
251 for the hydrolytic activity of Sle1 (M292I and G315C), two resulted in truncated versions of Sle1
252 (Q197* and V5*), while the last one acquired an alteration in the Shine-Dalgarno sequence of
253 *sle1* (G>A in the RBS). The mutations thus likely resulted in inactivation and/or reduced activity
254 of Sle1 (see below).

255

256 To further confirm that the growth defects caused by a lack of CxaR can be rescued by the
257 absence of *sle1*, *sle1* was knocked down in the Δ*cxaR* strain (**S7 Fig**). As expected, depletion
258 of Sle1 in the *cxaR* mutant resulted in loss of the biphasic growth and thus a reversion to a
259 wild type-like growth phenotype (**S7 Fig**).

260

261 **Sle1 levels are highly elevated in the absence of CxaR and reduced upon CxaR**
262 **overexpression**

263 To investigate the apparent functional link between CxaR and Sle1 levels, we performed
264 Western blot analyses using an antibody that recognizes Sle1 (35.8 kDa) [20]. Strikingly, a
265 clear accumulation of Sle1 was detected in cells lacking CxaR (Δ*cxaR* and *cxaR*$_{down}$ in **Fig. 5,**
266 **S8 Fig, S9 Fig**). Sle1 accumulation was observed both in the cell wall fraction, the extracellular
267 fraction, and the whole cell lysate. In contrast, when CxaR is overexpressed, Sle1 completely
268 disappears in all fractions (**Fig. 5, S8 Fig, S9 Fig**). Thus, the cellular levels of Sle1 are
269 controlled by CxaR, as both its presence and absence directly correlate with Sle1 protein
270 levels.
271
272 We then performed immunoblot assays with cell wall-associated and extracellular protein
273 extracts from the *cxaR* suppressor mutants (**Fig 4D**). This revealed reduced levels of cell wall-
274 associated Sle1 in cells with the *sle1* RBS mutation as well as in those encoding truncated
275 Sle1 versions, compared to the wild-type. The mutants with single CHAP-domain substitutions
276 also exhibited slightly reduced Sle1 levels, although not restored to wild-type levels. This
277 further supports the notion that reducing Sle1 levels or activity can compensate for the loss of
278 CxaR.
279
280 Given that reduced levels of Sle1 seem to rescue growth of cells lacking CxaR, we investigated
281 whether the same mechanism was at play when growth was restored at high temperatures
282 and/or with the addition of penicillin G. Indeed, both treatment with penicillin G and incubation
283 at 42°C reduced Sle1 levels, both in wild-type cells and cells without CxaR (**S10A-B Fig**). We
284 also tested whether the other antibiotics that stimulated growth of the *cxaR*$_{down}$ mutant had a
285 similar effect on Sle1 levels (**Fig 1D**). Indeed, a reduction in cell wall-associated Sle1 was
286 observed, although the extent of reduction varied. Oxacillin, bacitracin, moenomycin,
287 tunicamycin, and kanamycin all appeared to decrease Sle1 levels in the Δ*cxaR* strain to some
288 degree. However, for teicoplanin and novobiocin, the effect on Sle1 levels was less evident
289 (**S10C Fig**), consistent with their comparable limited ability to rescue growth of the *cxaR*$_{down}$

290 mutant. Together, this suggests that the stimulatory effects of antibiotics observed for the
291 Δ*cxaR* strain at least partially can be explained by reduced levels of Sle1.
292
293 **CxaR regulates Sle1 levels in a ClpXP-dependent manner**
294 Previous studies have shown that the cellular levels of Sle1 are regulated by the ClpXP
295 protease complex [38, 39], and similarly, we observed a strong accumulation of Sle1 Δ*clpX*
296 cells and cells devoid of ClpXP complex formation ($ClpX_{I265E}$) (**Fig 5**, **Fig 6A**, **S9 Fig**). In fact,
297 *cxaR* mutant cells phenocopies *clpX* mutants to a large degree, including the observed
298 temperature-dependent growth defect and growth rescue by cell wall targeting antibiotics (**S11**
299 **Fig**) [39, 41, 44]. These parallels suggest that CxaR plays a role in the ClpXP-mediated Sle1
300 degradation. Notably, the level of Sle1 accumulation in cells lacking either ClpXP activity or
301 CxaR was comparable (**Fig 5**, **S9 Fig**). If CxaR was primarily involved in regulating *sle1*
302 expression, one would expect the combined loss of CxaR and ClpXP to produce a significantly
303 stronger Sle1 accumulation compared to either single mutant. However, $ClpX_{I265E}$ cells with
304 CxaR depletion showed no greater Sle1 accumulation than $ClpX_{I265E}$ cells (**S9 Fig**). In addition,
305 there was no reduction in cell wall-associated Sle1 when CxaR was overexpressed in the
306 Δ*clpX* mutant, indicating that the mechanism in which CxaR controls Sle1 levels is not active
307 when *clpX* is deleted (**S9 Fig**). Furthermore, a *cxaR clpX* double knockdown strain did not
308 exacerbate the phenotypes of the two single knockdowns (**S11A and C Fig**). Together, this
309 suggests that CxaR and ClpXP likely operate within a shared pathway rather than through
310 independent mechanisms.
311
312 **CxaR directly interacts with ClpXP and Sle1**
313 Seeing that structural modeling of CxaR suggests it may contain a TPR-like domain (**Fig 1E**)
314 commonly associated with protein-protein interactions [64, 66, 67], we investigated the
315 potential role of CxaR in mediating interactions between Sle1 and ClpXP. We employed the
316 split luciferase system [68], where the proteins of interest are conjugated to the complementary

317 small (SmBit) and large (LgBit) subunits of luciferase, which produce a quantifiable
318 luminescence signal if they come into close proximity when expressed in *S. aureus*.
319
320 Initially, CxaR self-interaction was tested, as TPR-containing proteins commonly exhibit self-
321 oligomerization when involved in regulatory roles [69, 70]. Indeed, CxaR appears to
322 oligomerize, as that the self-interaction displayed a significant 10-fold higher value than the
323 control (**Fig 6B**). Next, interactions between CxaR, ClpX, and ClpP were tested. Luminescence
324 readings between all three were highly significant (**Fig 6B-C**). While it is well established that
325 ClpX and ClpP form a proteolytic complex (**Fig 6A and C**), CxaR also appears to interact with
326 both proteins, displaying a 25-fold and 13-fold increase in signal compared to the control,
327 respectively (**Fig 6B**). However, the interaction between CxaR and ClpX appears to be lost
328 when ClpX contains the I265E mutation (**Fig 6C**), suggesting that CxaR only interacts with the
329 ClpXP complex. Notably, the interaction of CxaR with ClpX generated a stronger signal than
330 the interaction with ClpP.
331
332 Moreover, CxaR also displayed a significant interaction with the precursor of Sle1, with a 4-
333 fold increase in luminescence signal compared to the control (**Fig 6D-E**). Interestingly,
334 however, this interaction was not observed when Sle1 was expressed without the signal
335 peptide (**Fig 6D-E**). Indeed, in the AlphaFold3 predicted interaction model, supported by a high
336 interaction score, the first LysM domain of Sle1 (located in the N-terminal part close to the
337 signal sequence) interacts with the predicted binding groove of CxaR (**Fig 1E**, **S12 Fig**).
338 Neither the precursor nor the mature form of Sle1 showed any detectable interaction with ClpX
339 (**Fig 6F**). Together this strongly suggests that CxaR functions as an adaptor or intermediary to
340 mediate the interaction between Sle1 and the ClpXP complex, facilitating Sle1 degradation.
341 Since the Sle1 precursor is transported across the cytoplasmic membrane via its N-terminal
342 signal peptide (**Fig 6D**), it is expected that only the precursor of Sle1 is accessible for
343 degradation by the cytoplasmic ClpXP complex.
344

345 **CxaR localization is ClpX-dependent**

346 ClpX has been shown to localize in single foci near the membrane, positioned close to the
347 ingrowing septum, in *S. aureus* cells undergoing septation [45]. This was confirmed here by
348 expressing an inducible ClpX-mCherry fusion (**S13A Fig**). Furthermore, a CxaR-GFP fusion
349 appeared to localize at midcell in dividing cells (**Fig 7A**, **S13B-C Fig**). Indeed, when co-
350 expressing ClpX-mCherry and CxaR-GFP, a clear co-localization of the two proteins was
351 observed, with their fluorescent signals appearing at the exact same positions in approximately
352 92% of cells (n = 635) (**Fig 7C and D)**. To determine whether CxaR depends on ClpX for its
353 localization, a plasmid encoding CxaR-GFP was transformed into the Δ*clpX* mutant. In these
354 cells, the distinct signal pattern was lost (**Fig 7F**), suggesting that CxaR requires ClpX for its
355 spatiotemporal localization. However, when ClpX-mCherry was introduced into Δ*cxaR* cells,
356 the localization remained unchanged (**Fig 7E**), indicating that ClpX localization is independent
357 of CxaR. It should be noted that while the CxaR-GFP fusion seems to be functional in terms of
358 growth (**Fig 7B**), cells expressing CxaR-GFP, either from its native promoter on the
359 chromosome or from a plasmid, exhibited cell separation defects, including cell clumping (**Fig
360 7A**, **S13B-C Fig**).

361 ## Discussion

362 In this work, we have discovered a novel factor critical for regulating cell splitting in *S. aureus*.
363 Our results demonstrate that the hitherto unstudied protein CxaR acts as an adaptor protein,
364 controlling the levels of Sle1, a PGH crucial for staphylococcal cell separation. Specifically, our
365 model proposes that CxaR binds the Sle1 precursor prior to its export and translocates it to
366 the ClpXP protease for degradation (**Fig 8**).

367

368 This model is supported by several experimental observations. First, we observed that *cxaR*
369 mutants phenocopies *clpX* mutants in a number of aspects, including biphasic growth profiles,
370 temperature-dependent growth phenotypes with exacerbation of the growth defect at
371 suboptimal and improved growth at supraoptimal temperatures [44], high lysis frequency due
372 to premature cell splitting [41], and accumulation of Sle1 [38]. These defects were found to be
373 alleviated by certain antibiotics, including β-lactams and tunicamycin, as well as inactivation of
374 Sle1, similar to what has previously been observed for cells lacking ClpX [41]. Consistently,
375 overexpression of CxaR led to depletion of cellular Sle1 due to enhanced degradation, causing
376 severely impaired cell splitting. Second, split luciferase assays, used to assess protein-protein
377 interactions *in vivo*, showed that CxaR interacts directly with the ClpXP complex, as well as
378 Sle1. However, no direct interaction between Sle1 and ClpX was detected in these assays,
379 suggesting that an intermediate protein facilitates the delivery of Sle1 to ClpXP for targeted
380 degradation. Third, subcellular localization analysis showed that CxaR co-localizes with ClpX
381 near the septum in dividing *S. aureus* cells. Additionally, the localization of CxaR was
382 dependent on the presence of ClpX, indicating that its function is closely linked to ClpX and
383 likely cell division. Moreover, it should also be noted that CxaR exhibited the highest score
384 among identified staphylococcal ClpXP substrates when a proteolytically inactive ClpP variant
385 ($ClpP^{trap}$) was expressed *in vivo* in *S. aureus* [38]. However, CxaR-GFP does not appear to
386 accumulate in *S. aureus* cells lacking ClpXP activity (**S13D Fig**), suggesting that its retention
387 in the $ClpP^{trap}$ is likely due to other interactions than direct degradation. Finally, structural

388 analyses revealed that CxaR resembles proteins containing TPR motifs, which are typically
389 involved in facilitating protein-protein interactions [64, 66, 67]. This structural similarity
390 suggests that CxaR may bind specific substrates to mediate their interactions or delivery. Thus,
391 dysregulation of CxaR levels have detrimental effects on cell splitting and growth; Sle1
392 accumulates in the absence of CxaR, resulting in cell lysis due to premature splitting, while
393 high levels of CxaR, on the other hand, significantly delay cell splitting, leading to cell clumping
394 and cells with multiple septa, by reducing Sle1 abundances.
395
396 *cxaR* was uncharacterized prior to this study, but its transcription has been shown to increase
397 under various stress conditions, including treatment with vancomycin [71], oxacillin [72],
398 mersacidin [73], brilacidin [74], and under heat shock [75]. This pattern of transcriptional
399 upregulation in response to envelope damage is consistent with the finding that expression of
400 *cxaR* likely is regulated by the two-component system VraSR (vancomycin-resistance
401 associated sensor/regulator). VraSR is activated by cell wall targeting antimicrobials, such as
402 β-lactams and glycopeptides, and controls transcriptional induction of several cell wall-
403 associated genes [72, 76]. While Sle1 and other PGHs are not directly regulated by the VraSR
404 system, it can thus be speculated that VraSR-mediated upregulation of CxaR serves as a
405 regulatory mechanism to reduce Sle1 levels under these conditions, thereby delaying cell
406 splitting in response to cell wall stress. This delay could provide the cells with enough time to
407 repair damaged peptidoglycan and reinforce cell wall integrity, ultimately enhancing bacterial
408 survival.
409
410 While our results show that CxaR regulates Sle1 levels via ClpXP-mediated degradation, it
411 may have additional roles in the cell that remain to be elucidated. For example, when
412 performing localization microscopy with fluorescently tagged versions of CxaR, we surprisingly
413 observed that overexpression of CxaR-GFP in Δ*clpX* appeared to improve growth of the
414 deletion strain (**Fig 7E**). This was also confirmed with a non-tagged CxaR in the *clpX* deletion
415 mutant (**S14 Fig**). Western blot assays did not indicate any decrease in cell wall-associated

416 Sle1 during CxaR overexpression in Δ*clpX* cells (**S9 Fig**), which suggests that CxaR may have
417 an additional role which helps the cells mitigate the impact of elevated Sle1 levels, potentially
418 by rendering Sle1 non-functional. Additionally, the CxaR overexpression phenotype appears
419 to be more severe than the expected defects from *sle1* deletion alone [2, 7, 9, 10], more closely
420 resembling mutants with deletions of several PGHs [9, 77]. This could indicate an additional
421 role of CxaR in cell division, or that CxaR facilitates ClpXP-mediated degradation of other
422 proteins in addition to Sle1.
423
424 Sublethal concentrations of different antibiotics could rescue the growth defects observed in
425 *cxaR* mutants, a phenomenon previously reported in *clpX* mutants [41]. For some antibiotics,
426 the growth rescue can be directly attributed to reduced levels of Sle1 in the treated cells (**S10B-**
427 **C Fig**). This is in line with previous observations that expression of certain PGHs, including
428 *sle1,* is positively correlated with PBP transpeptidase activity [55, 56]. The reduction in Sle1
429 levels upon beta-lactam exposure is independent of *mecA*, as the same occurs in both MRSA
430 (JE2) and non-MRSA (NCTC8325-4) strains [7]. Sle1 levels are also highly temperature
431 dependent, increasing at 30°C and decreasing at temperatures exceeding 40°C [20]. The
432 temperature-dependent growth phenotype of cells lacking CxaR is likely attributed to these
433 fluctuating Sle1 levels. The exact mechanism by which temperature influences the levels of
434 Sle1 is unknown, but the observed upregulation of CxaR under heat [75] and envelope stress
435 [72, 76] suggest that elevated temperatures may enhance CxaR abundances, leading to
436 increased Sle1 degradation.
437
438 Beyond the direct impact antibiotics have on hydrolase activity, additional mechanisms are
439 likely involved in the antibiotic-mediated growth rescue of *cxaR* mutants. The growth
440 stimulation mediated by sublethal concentrations of tunicamycin may be attributed to the role
441 of teichoic acids in directing septal hydrolysis, in addition to its effect on Sle1 levels. A decrease
442 in wall teichoic acid abundance has been shown to reduce septum-directed localization of
443 PGHs and thus delay septal resolution [11, 15, 78, 79]. The same growth-rescue by

444 tunicamycin has also been observed in a Δ*clpX* mutant [41], which additionally acquired
445 spontaneous, growth-rescuing loss-of-function mutations in the gene encoding the lipoteichoic
446 acid synthase, *ltaS* [42]. Furthermore, sublethal concentrations of β-lactams have been
447 observed to prolong the duration of peptidoglycan biosynthesis at the septal wall, leading to
448 cells with thickened, unresolved septa, due to the retention of septal PBPs [41, 53, 54]. A
449 thicker septum could potentially mitigate the effects of increased autolytic activity caused by
450 Sle1 accumulation in *cxaR* mutants.
451
452 *S. aureus* employs a complex network of regulatory mechanisms to effectively control the
453 autolytic activity driving cell splitting. Given the important role of Sle1 in septum resolution, our
454 findings establish CxaR as a key regulatory factor in maintaining the balance between
455 peptidoglycan synthesis and hydrolysis – a balance which is critical to the function of
456 antibiotics. As CxaR represents a previously unrecognized component in this process, further
457 studies investigating its potential additional roles, as well as functional analogs in other
458 species, may provide new insight into the mode of action of widely used antibiotic classes,
459 including β-lactams.

460 # Materials and methods

461

462 **Bacterial strains and growth conditions**

463 Strains used in this work are listed in **S3 Table**. All *S. aureus* strains were grown in tryptic soy
464 broth (TSB) and *E. coli* strains were grown in lysogeny broth (LB) aerobically at 37°C, unless
465 stated otherwise. Growth in liquid media was carried out in an orbital shaker at 180 rpm, while
466 for growth on solid media 1.5% (w/v) agar was added to the respective medium base. When
467 appropriate, the following antibiotics were added for selection: ampicillin (Amp, 100 µg/mL),
468 chloramphenicol (Cam, 10 or 25 µg/mL), spectinomycin (Spc, 100 or 1,000 µg/mL for
469 NCTC8325-4 and JE2, respectively), and erythromycin (Ery, 5 µg/mL). In addition, isopropyl
470 β-D-1-thiogalactopyranoside (IPTG) or anhydrotetracycline (aTc) was added for induction of
471 gene expression when needed.

472

473 For *E. coli* transformation, chemically competent IM08B cells were prepared using calcium
474 chloride treatment, followed by heat shock transformation according to standard protocols.
475 Plasmids isolated from *E. coli* IM08B were transformed into electrocompetent *S. aureus* by
476 electroporation, as previously described [80].

477

478 **Strain and plasmid construction**

479 See **S3, S4 and S5 Tables** for strains, plasmids, and oligonucleotides used in this work. Every
480 construct was verified by PCR and sequencing.

481

482 *Construction of CRISPRi knockdown strains*

483 For gene knockdown, we used the two-plasmid CRISPR interference (CRISPRi) system
484 described previously [59, 81, 82]. In this system, dCas9 is expressed from an IPTG-inducible
485 promoter on the plasmid pLOW-*dcas9*, while the gene-specific single guide RNA (sgRNA) is
486 constitutively expressed from a second plasmid (pCG248-sgRNA(*x*) or pVL2336-sgRNA(*x*),
487 where *x* denotes the targeted gene). Upon co-expression, the dCas9-sgRNA complex binds

488 the gene of interest thereby blocking transcription by the RNA polymerase. The sgRNA
489 plasmids were constructed using inverse PCR for pCG248 [81] or Golden Gate cloning for
490 pVL2336 [59], with the oligonucleotide primers listed in **S5 Table**.
491
492 *Construction of the cxaR deletion mutant*
493 *cxaR* was replaced by a spectinomycin resistance cassette in its native loci in *S.*
494 *aureus* NCTC8325-4 using the temperature-sensitive pMAD system. First, the pMAD-
495 *cxaR*::*spc* plasmid was constructed by assembling a fragment containing the *cxaR* up- and
496 downstream regions (amplified using primer pairs mk591/mk592 and mk593/mk594,
497 respectively) flanking a spectinomycin resistance cassette (amplified from pCN55 with primers
498 mk188 and mk189) using overlap extension PCR. The fragment was ligated into pMAD using
499 restriction cloning with NcoI and BamHI, and the resulting plasmid was transformed into *E. coli*
500 IM08B. Construction of Δ*cxaR*::*spc* in strain NCTC8325-4 was then performed using a
501 standard pMAD protocol with temperature shifts, as described before [83].
502
503 *Construction of suppressor mutants*
504 When the NCTC8325-4 *cxaR* deletion mutant was plated at 30°C, larger colonies consistently
505 appeared among the very small colonies observed at 37°C. To determine whether these larger
506 colonies had restored growth due to acquisition of spontaneous suppressor mutations, we
507 performed a genetic suppressor screen similar to what has been described previously [42].
508 The Δ*cxaR* mutant was streaked for single colonies on TSA plates and incubated at 37°C
509 overnight. Single small colonies were picked, resuspended in TSB, and grown overnight at
510 37°C with shaking. The following day, each independent overnight culture was plated on TSA
511 and incubated overnight at 30°C. On some plates, visibly larger colonies had appeared. In
512 those cases, a single large colony from each independent culture was selected, grown
513 overnight in TSB at 30°C with shaking, and stored. For cultures without initially detectable
514 larger colonies, a random colony was picked, grown overnight in TSB at 30°C, and then
515 replated on TSA at 30°C. By the next day, all plates had a majority of large colonies. One large

516 colony per plate was picked, grown overnight in TSB at 30°C, and stored. The growth of the
517 stored cultures was analyzed, and five were selected for whole-genome re-sequencing.
518
519 *Construction of plasmids for complementation and overexpression*
520 *cxaR* and *clpX* were amplified from *S. aureus* genomic DNA using the primer pairs
521 mhu28/mhu27 and mdb98/mdb99, respectively. The resulting fragments were digested with
522 SalI and EcoRI and subsequently ligated into the corresponding restriction sites of plasmid
523 pLOW-*m(sf)gfp-SA1477* to produce pLOW-*cxaR* and pLOW-*clpX*, which enable IPTG-
524 inducible expression of the respective genes.
525
526 *Construction of plasmids for localization analysis of CxaR and ClpX*
527 To study the subcellular localization of C-terminally tagged CxaR, *cxaR* was amplified from *S.*
528 *aureus* genomic DNA using primers mhu28 and mhu29, digested with SalI and BamHI, and
529 ligated into the respective sites of pLOW-*SA0948-m(sf)gfp*. For N-terminally tagged CxaR,
530 *cxaR* was amplified from *S. aureus* genomic DNA using primers mhu26 and mhu27, digested
531 with BamHI and EcoRI, and ligated into the respective sites of pLOW-*m(sf)gfp-SA1477*. To
532 study the subcellular localization of C-terminally tagged ClpX, *clpX* was amplified from *S.*
533 *aureus* genomic DNA using primers mdb98 and mdb102, digested with SalI and BamHI, and
534 ligated into the respective sites of pLOW-*lacA-mCherry*.
535
536 *Construction of a chromosomally integrated cxaR-m(sf)gfp fusion*
537 The temperature-sensitive pMAD system was used to GFP-tag *cxaR* in its native loci in *S.*
538 *aureus* NCTC8325-4. To construct pMAD-*cxaR-m(sf)gfp_spc* the following four fragments
539 were amplified: (1) the upstream region of *cxaR* with primers mdb58 and mdb59 using gDNA
540 from *S. aureus* NCTC8325-4 as a template, (2) the *cxaR-m(sf)gfp* fusion from plasmid pLOW-
541 *cxaR-m(sf)gfp* using primers mdb60 and mdb61, (3) the spectinomycin resistance cassette
542 using primers mk503 and mk504 from plasmid pCN55, and (4) the downstream region of *cxaR*
543 from *S. aureus* NCTC8325-4 gDNA using mdb62 and mdb63. These fragments were

544 subsequently fused by overlap extension PCR and ligated into pMAD using the NcoI and SalI
545 restriction sites introduced by the outer primers. Finally, chromosomal integration of the fusion
546 construct was performed following a standard pMAD protocol [84].
547
548 *Construction of split luciferase plasmids*
549 To C-terminally fuse CxaR, ClpX, and $ClpX_{I265E}$ to the small luciferase subunit
550 (SmBit), *cxaR*, *clpX*, and $clpX_{I265E}$ were amplified from *S. aureus* NCTC8325-4 WT or $clpX_{I265E}$
551 genomic DNA using the primer pairs efs7/efs8 for *cxaR* and mdb93/mdb94 for *clpX*
552 and $clpX_{I265E}$. The amplified fragments and vectors pAF256-P_{tet}-*hupA-smbit*/*lgbit* and pAP118-
553 P_{tet}-*hupA-smbit*/*hupA-lgbit* were then digested with SacI and XhoI. The digested fragments
554 were ligated into the vectors and subsequently transformed into *E. coli* IM08B. The pAF256
555 vectors, encoding CxaR, ClpX, or $ClpX_{I265E}$ fused to SmBit and LgBit not part of a fusion
556 protein, served as negative controls in the split luciferase assays. The pAP118 vectors were
557 further modified to C-terminally fuse CxaR, ClpX, ClpP, Sle1, or Sle1 (without signal peptide)
558 to the large luciferase subunit (LgBit). All fragments were amplified using NCTC8325-4 WT
559 genomic DNA as template and the following primer pairs: (1) efs20/efs21 for *cxaR*, (2)
560 efs5/efs6 for *clpX*, (3) efs9/efs10 for *clpP*, (4) mdb88/mdb89 for *sle1*, and (5) mdb90/mdb89
561 for *sle1* (without signal peptide). The amplified fragments and the corresponding pAP118
562 vectors were then digested with PvuI and NotI, ligated, and subsequently transformed into *E.*
563 *coli*.
564
565 **Genome re-sequencing and analysis**
566 Whole-genome sequencing of Δ*cxaR* (MK2047), the strain expressing chromosomally
567 integrated CxaR-GFP (MDB376), and the *cxaR* suppressor mutants (EFS104, EFS105,
568 MDB390, MDB401, and MDB404) was performed. Genomic DNA was isolated from the
569 respective strains using The Wizard Genomic DNA Purification Kit (Promega) and sent to
570 Novogene for Illumina sequencing. Sequence assembly to the reference genomes and SNP
571 detection were done using Geneious Prime [85].

572

573 **CRISPRi-sequencing screen**

574 The explorative CRISPRi-seq screen for penicillin G susceptibility determinants was performed
575 as described before, using an already constructed genome-wide CRISPRi library in the *S.*
576 *aureus* strain NCTC8325-4 [59, 60]. Briefly, the library (pre-grown in BHI to OD_{600} = 0.8) was
577 diluted 1:1,000 in 100 mL ultra-high temperature (UHT) treated milk (Tine SA, Norway) and
578 incubated at 37 °C with shaking for 7 hours. After, it was reinoculated 1:1,000 in fresh UHT
579 milk and grown for another 6 hours. Chloramphenicol (10 µg/mL) was added for selection, and
580 when appropriate, 30 ng/mL anhydrotetracycline was added for induction of the CRISPRi-
581 system. Furthermore, to identify fitness determinant affected by β-lactam treatment, the library
582 was grown in the presence and absence of 0.008 µg/mL penicillin G (corresponding to the MIC
583 for NCTC8325-4 in milk). Four parallels were included per condition. After growth, cells were
584 harvested by centrifugation, and plasmids were isolated as previously described [60]. Illumina
585 amplicon libraries were prepared, and sequencing was performed on a NovaSeq platform
586 using 150 bp paired-end reads (performed by Novogene, UK) following established protocols
587 [60]. CRISPRi-seq differential enrichment analyses was done as described by Bakker et al.
588 [58] and Mårli et al. [60]. Notably, due to the inhibitory concentration of penicillin G used in this
589 explorative screen, the number of generations for growth of the penicillin G treated library was
590 significantly lower than for the untreated library.

591

592 **Growth assays in liquid media**

593 To assess bacterial growth in a liquid medium, overnight cultures of the strains to be monitored
594 were diluted 1:1,000 in TSB medium supplemented with the appropriate antibiotics and
595 inducers. For MIC analysis, the following panel of antibiotics were tested against the JE2 *cxaR*
596 knockdown mutant and CRISPRi control strain in two-fold dilution series: penicillin G (PEN),
597 oxacillin (OXA), cefoxitin (CXI), vancomycin (VAN), teicoplanin (TEC), bacitracin (BAC),
598 moenomycin (MOE), tunicamycin (TUN), ciprofloxacin (CIP), novobiocin (NOV), trimethoprim
599 (TMP), rifampicin (RIF), erythromycin (ERY), kanamycin (KAN), and streptomycin (STR).

600 Bacterial dilutions were added to a 96-well microtiter plate and incubated in a plate reader at
601 37°C for 20 hours, unless otherwise stated. OD_{600} measurements were taken every 10
602 minutes, with a brief shaking of the plate for 5 seconds prior to each measurement. All growth
603 curves in this work are the mean of three replicate measurements, with the exception of the
604 MIC panel (**S3 Fig**), growth at different temperatures (**S6A Fig**), and CxaR/ClpX
605 overexpression (**S14 Fig**) which represent the mean value of two replicates, and they are all
606 representative of at least two independent experiments.
607

608 **Spotting assays**

609 Overnight cultures diluted 1:1,000 in TSB with the appropriate antibiotics were grown at 37°C
610 until they reached an OD_{600} of 0.5 or the indicated time point. The cultures were diluted in a
611 ten-fold dilution series from 10^{-1} to 10^{-8} and 5 µL from each dilution was spotted on TSA. The
612 TSA, in addition to the appropriate selective antibiotics, contained 500 µM IPTG for CRISPRi
613 knockdown strains and 1 ng/mL penicillin G or 6 ng/mL oxacillin when assessing growth rescue
614 by β-lactams. The plates were incubated for 24 hours at their indicated temperature. All
615 presented spotting assays are representative of three technical replicates from at least three
616 independent experiments.
617

618 **Western blot analyses of Sle1 levels**

619 *Cell harvesting*

620 Overnight cultures were diluted 1:1,000 in TSB medium with the appropriate antibiotics and
621 inducers and incubated at either 37°C or 42°C with shaking until an OD_{600} of approximately
622 0.4 was reached.
623

624 *Preparation of extracellular and cell wall-associated protein extracts*

625 Culture volumes of 50 mL were harvested by centrifugation at 6,000 x *g* for five minutes at 4°C.
626 To extract extracellular proteins, 30 mL of the supernatants were mixed with 30 mL 96%

627 ethanol and incubated overnight at 4°C. To extract cell wall-associated proteins, the pellets
628 were washed with 10 mL cold 0.9% (w/v) NaCl and centrifuged at 6,000 x *g* at 4°C for five
629 minutes. The supernatants were discarded, and cell wall-associated proteins were eluted with
630 10 mL 4% (w/v) SDS at 25°C for 45 minutes with shaking. The samples were then centrifuged
631 at 6,000 x *g* for five minutes at 4°C, and the resulting supernatants were mixed with 10 mL
632 96% ethanol and left to precipitate at 4°C overnight. The following day, the protein extracts
633 were pelleted by centrifugation at 10,000 x *g* for 30 minutes at 4°C, dried in a fume hood, and
634 normalized with 50 mM Tris-HCl (pH 7.4). The normalized extracts were mixed 1:1 with 2x
635 SDS loading buffer and heated at 95°C for five minutes prior to SDS-PAGE.
636
637 *Preparation of whole cell lysate*
638 Culture volumes of 50 mL, normalized to an OD_{600} of 0.4, were harvested by centrifugation at
639 4,000 x *g* for five minutes at 4°C. The pellets were resuspended in 100 µL TBS buffer and
640 mechanically lysed using the Fast Prep method with ≤106 µm glass beads in three cycles of
641 20 seconds at 6 m/s, with one minute incubation on ice between cycles. Insoluble material
642 was removed by centrifugation at 20,000 × g for 2 minutes. Next, the supernatants were
643 mixed with equal volumes 2x SDS loading buffer and heated at 95°C for 5 minutes prior to
644 SDS-PAGE.
645
646 *SDS-PAGE, Western blotting, and detection*
647 The protein samples were separated by SDS-PAGE on a polyacrylamide gel, which consisted
648 of a 12% separation gel with a 4% stacking gel layered on top. The proteins were then
649 electroblotted onto a PVDF membrane using the Trans-Blot Turbo System (Bio-Rad).
650 Afterward, the membrane was trimmed to retain proteins below 60 kDa and blocked in TBST,
651 containing 5% (w/v) bovine serum albumin (BSA) and 1 µg/mL human IgG, for 1 hour at room
652 temperature, followed by overnight incubation at 4°C. After washing the membrane with TBST,
653 the following day, it was incubated with an anti-Sle1 primary antibody [20] (diluted 1:10,000 in

654 TBST with 2% (w/v) BSA and 1 µg/mL human IgG) for 1 hour. Next, unbound antibodies were
655 removed by three TBST washes, and the membrane was then incubated for another hour with
656 an anti-mouse IgG HRP-conjugate secondary antibody (Promega) (diluted 1:10,000 in TBST
657 with 1 µg/mL human IgG). After another series of washes, the membrane was finally developed
658 using the SuperSignal West Pico PLUS Chemiluminescent Substrate kit (Thermo Fisher
659 Scientific), and blot images were captured with an Azure Imager c400 (Azure Biosystems).
660

661 **Western blot analysis of GFP-tagged CxaR**

662 Overnight cultures of MDB376 (NCTC8325-4 with a chromosomally integrated *cxaR-*
663 *m(sf)gfp* fusion), MDB430 (NCTC8325-4 carrying pLOW-*cxaR-m(sf)gfp*), and MDB395
664 (NCTC8325-4 $clpX_{I265E}$ carrying pLOW-*cxaR-m(sf)gfp*) were diluted 1:1,000 in TSB medium
665 supplemented with 100 µg/mL spectinomycin (for MDB376) or 5 µg/mL erythromycin and 10
666 µM IPTG (for MDB430 and MDB395). The bacterial cultures were incubated at 37°C until they
667 reached an OD_{600} of approximately 0.5 and 1. They were then normalized to an OD_{600} of 0.5,
668 and harvested by centrifugation at 4,000 × *g* for 5 minutes at 4°C. The pellets were
669 resuspended in 200 µL TBS buffer and lysed mechanically using the Fast Prep method with
670 ≤106 µm glass beads at 6 m/s for three cycles of 20 seconds each. Insoluble material was
671 removed by centrifugation at 20,000 × g for 2 minutes. Next, the supernatants were mixed with
672 equal volumes 2x SDS loading buffer and heated at 95°C for 5 minutes.

673 The subsequent SDS-PAGE, blotting, and GFP detection were performed as described above
674 for Sle1 immunoblotting, with the exception of antibody selection. GFP-tagged CxaR was
675 detected using an anti-GFP primary antibody (Invitrogen) (diluted 1:4,000 in TBST) and an
676 anti-rabbit IgG HRP-conjugated secondary antibody (Promega) (diluted 1:5,000 in TBST).
677
678
679
680

681 **Phase contrast and epifluorescence microscopy**

682 *Microscopy*

683 Overnight cultures were diluted 1:1,000 in TSB medium with the appropriate antibiotics and
684 inducers. These cultures were incubated at 37°C with shaking until they reached the desired
685 optical density (OD_{600} ~0.4) or time point, followed by cooling on ice. In some cases, cells were
686 then stained with fluorescent vancomycin (VanFL, 0.8 µg/mL [Invitrogen]) to visualize the cell
687 wall and/or 4′,6-diamidino-2-phenylindole (DAPI, 7.5 µg/mL [Invitrogen]) to visualize the
688 nucleoid. Bacterial cells were immobilized on 1.2% (w/v) agarose pads before imaging on
689 either a Zeiss Axio Observer microscope or a Leica DMi8 microscope. The bacteria were
690 visualized with a 100× phase contrast objective, and images were captured using an ORCA-
691 Flash4.0 V3 Digital CMOS (for the Zeiss microscope) or a K8 Scientific CMOS (for the Leica
692 microscope) camera.

693

694 *Image analysis*

695 Cell size distribution among different *S. aureus* strains was determined using MicrobeJ [86].
696 Bacterial cells were automatically detected using phase contrast image stacks, and every
697 image was subsequently manually corrected by adding unidentified cells or removing
698 incorrectly identified cells. Additionally, co-localization of CxaR-GFP and ClpX-mCherry was
699 analyzed manually by examining both signals in 300–350 randomly selected cells from two
700 biological replicates (n = 635).

701

702 **Transmission electron microscopy**

703 Overnight cultures of the NCTC8325-4 *cxaR* CRISPRi knockdown and control strains were
704 diluted 1:1,000 in 10 mL TSB with the appropriate selective antibiotics and inducers, with and
705 without 1 ng/mL penicillin G. The cultures were grown at 37°C for 11 hours, corresponding to
706 the transient minimum of the *cxaR* knockdown strain. The cultures were added to fixative to a
707 final concentration of 1.25% (v/v) glutaraldehyde, 2% (v/v) paraformaldehyde, and 100 mM
708 cacodylate (CaCo) buffer. The cells were fixed for one hour at room temperature and overnight

709 at 4°C, before being washed in 100 mM CaCo buffer three times. The final pellets were
710 embedded in 3% (w/v) low-melt agarose and stored in 100 mM CaCo buffer. Post-fixation with
711 1% osmium tetroxide was performed for one hour. Excess osmium tetroxide was removed by
712 washing with 100 mM CaCo buffer and the pellets were dehydrated using gradually increasing
713 concentrations of cold acetone. The dehydrated pellets were embedded in EPON epoxy resin
714 and polymerized at 60°C. The samples were sectioned 60 nm thick and stained with uranyl
715 acetate and lead citrate. A Jeol JEM-2100Plus was used for imaging.
716

717 **Split luciferase assays**

718 Pairwise protein-protein interactions were assessed *in vivo* in *S. aures* NCTC8325-4 using the
719 split luciferase system developed by Paiva et al. [68] for *C. difficile*, following the same
720 approach as described before [87].
721

722 **Structural and phylogenetic analysis**

723 The presence of general structural features, including transmembrane helices and signal
724 peptides, were predicted using SignalP-6.0 and DeepTMHMM [88, 89]. Homologs of CxaR
725 within *Staphylococcaceae* were identified through BLASTp, using the NCTC8325-4 CxaR
726 peptide sequence as the query [90]. Sequence representatives from 55 species within
727 *Staphylococcus*, *Mammaliicoccus*, and *Macrococcus* were aligned by Clustal Omega, and the
728 multiple sequence alignment (MSA) was visualized using Jalview [91, 92]. Phylogenetic trees
729 from the homologs were generated using MEGA11 [93]. HMMER and HHpred were applied
730 for sensitive hidden Markov model-based homolog searches to detect structural motifs [61,
731 62]. TPRpred from the HH-suite was used to detect TPR-like motifs in CxaR homologs [94].
732

733 ***In silico* protein interaction modelling**

734 AlphaFold 3 [95] was used for the modelling of every protein structure and protein interactions
735 in this work. The top ranked predictions were selected and visualized using either ChimeraX
736 [96] or PyMOL [97].

Acknowledgements

We would like to thank the NMBU Imaging Center for help with TEM, and Zhian Salehian and Anne Ohren Nordraak at NMBU for laboratory assistance.

References

1. Zhou X, Halladin DK, Rojas ER, Koslover EF, Lee TK, Huang KC, et al. Mechanical crack propagation drives millisecond daughter cell separation in *Staphylococcus aureus*. Science. 2015;348(6234):574-8. doi: 10.1126/science.aaa1511.
2. Monteiro JM, Fernandes PB, Vaz F, Pereira AR, Tavares AC, Ferreira MT, et al. Cell shape dynamics during the staphylococcal cell cycle. Nat Comm. 2015;6(1):8055. doi: 10.1038/ncomms9055.
3. Barbuti MD, Myrbråten IS, Morales Angeles D, Kjos M. The cell cycle of *Staphylococcus aureus*: An updated review. Microbiol Open. 2023;12(1):e1338. doi: 10.1002/mbo3.1338.
4. Matias VRF, Beveridge TJ. Cryo-electron microscopy of cell division in *Staphylococcus aureus* reveals a mid-zone between nascent cross walls. Mol Microbiol. 2007;64(1):195-206. doi: 10.1111/j.1365-2958.2007.05634.x.
5. Wang M, Buist G, van Dijl JM. *Staphylococcus aureus* cell wall maintenance – the multifaceted roles of peptidoglycan hydrolases in bacterial growth, fitness, and virulence. FEMS Microbiol Rev. 2022;46(5). doi: 10.1093/femsre/fuac025.
6. Vollmer W, Joris B, Charlier P, Foster S. Bacterial peptidoglycan (murein) hydrolases. FEMS Microbiol Rev. 2008;32(2):259-86. doi: 10.1111/j.1574-6976.2007.00099.x.
7. Thalsø-Madsen I, Torrubia FR, Xu L, Petersen A, Jensen C, Frees D. The Sle1 Cell Wall Amidase Is Essential for β-Lactam Resistance in Community-Acquired Methicillin-Resistant *Staphylococcus aureus* USA300. Antimicrob Agents Chemother. 2019;64(1):10.1128/aac.01931-19. doi: 10.1128/aac.01931-19.
8. Wang M, Li X, Cavallo FM, Yedavally H, Piersma S, Raineri EJM, et al. Functional profiling of CHAP domain-containing peptidoglycan hydrolases of *Staphylococcus aureus* USA300 uncovers potential targets for anti-staphylococcal therapies. Intl J Med Microbiol. 2024;316:151632. doi: 10.1016/j.ijmm.2024.151632.
9. Kajimura J, Fujiwara T, Yamada S, Suzawa Y, Nishida T, Oyamada Y, et al. Identification and molecular characterization of an N-acetylmuramyl-l-alanine amidase Sle1 involved in cell separation of *Staphylococcus aureus*. Mol Microbiol. 2005;58(4):1087-101. doi: 10.1111/j.1365-2958.2005.04881.x.
10. Veiga H, Jousselin A, Schäper S, Saraiva BM, Marques LB, Reed P, et al. Cell division protein FtsK coordinates bacterial chromosome segregation and daughter cell separation in *Staphylococcus aureus*. EMBO J. 2023;42(11):e112140. doi: 10.15252/embj.2022112140.
11. Frankel MB, Schneewind O. Determinants of Murein Hydrolase Targeting to Cross-wall of *Staphylococcus aureus* Peptidoglycan. J Biol Chem. 2012;287(13):10460-71. doi: 10.1074/jbc.M111.336404.
12. Bateman A, Rawlings ND. The CHAP domain: a large family of amidases including GSP amidase and peptidoglycan hydrolases. Trends Biochem Sci. 2003;28(5):234-7. doi: 10.1016/S0968-0004(03)00061-6.
13. Uehara T, Parzych KR, Dinh T, Bernhardt TG. Daughter cell separation is controlled by cytokinetic ring-activated cell wall hydrolysis. EMBO J. 2010;29(8):1412-22. doi: 10.1038/emboj.2010.36.
14. Sham L-T, Barendt SM, Kopecky KE, Winkler ME. Essential PcsB putative peptidoglycan hydrolase interacts with the essential $FtsX_{Spn}$ cell division protein in *Streptococcus pneumoniae* D39. Proc Natl Acad Sci U S A. 2011;108(45):E1061-E9. doi: 10.1073/pnas.1108323108.
15. Schlag M, Biswas R, Krismer B, Kohler T, Zoll S, Yu W, et al. Role of staphylococcal wall teichoic acid in targeting the major autolysin Atl. Mol Microbiol. 2010;75(4):864-73. doi: 10.1111/j.1365-2958.2009.07007.x.
16. Delaune A, Poupel O, Mallet A, Coic Y-M, Msadek T, Dubrac S. Peptidoglycan Crosslinking Relaxation Plays an Important Role in *Staphylococcus aureus* WalKR-Dependent Cell Viability. PLoS One. 2011;6(2):e17054. doi: 10.1371/journal.pone.0017054.

17. Dubrac S, Bisicchia P, Devine KM, Msadek T. A matter of life and death: cell wall homeostasis and the WalKR (YycGF) essential signal transduction pathway. Mol Microbiol. 2008;70(6):1307-22. doi: 10.1111/j.1365-2958.2008.06483.x.
18. Delauné A, Dubrac S, Blanchet C, Poupel O, Mäder U, Hiron A, et al. The WalKR system controls major staphylococcal virulence genes and is involved in triggering the host inflammatory response. Infect Immun. 2012;80(10):3438-53. Epub 20120723. doi: 10.1128/iai.00195-12. PubMed PMID: 22825451; PubMed Central PMCID: PMCPMC3457574.
19. Falord M, Mäder U, Hiron A, Débarbouillé M, Msadek T. Investigation of the *Staphylococcus aureus* GraSR Regulon Reveals Novel Links to Virulence, Stress Response and Cell Wall Signal Transduction Pathways. PLoS One. 2011;6(7):e21323. doi: 10.1371/journal.pone.0021323.
20. Mebus VH, Busch LM, Børre M, Nielsen TK, Bojer MS, Henriksen C, et al. Temperature-dependent regulation of bacterial cell division hydrolases by the coordinated action of a regulatory RNA and the ClpXP protease. bioRxiv. 2025:2025.04.01.646552. doi: 10.1101/2025.04.01.646552.
21. Kirstein J, Molière N, Dougan DA, Turgay K. Adapting the machine: adaptor proteins for Hsp100/Clp and AAA+ proteases. Nat Rev Microbiol. 2009;7(8):589-99. doi: 10.1038/nrmicro2185.
22. Mahmoud SA, Chien P. Regulated Proteolysis in Bacteria. Ann Rev Biochem. 2018;87(Volume 87, 2018):677-96. doi: 10.1146/annurev-biochem-062917-012848.
23. Bouchnak I, van Wijk KJ. Structure, function, and substrates of Clp AAA+ protease systems in cyanobacteria, plastids, and apicoplasts: A comparative analysis. J Biol Chem. 2021;296:100338. doi: 10.1016/j.jbc.2021.100338.
24. Olivares AO, Baker TA, Sauer RT. Mechanistic insights into bacterial AAA+ proteases and protein-remodelling machines. Nat Rev Microbiol. 2016;14(1):33-44. doi: 10.1038/nrmicro.2015.4.
25. Levchenko I, Seidel M, Sauer RT, Baker TA. A Specificity-Enhancing Factor for the ClpXP Degradation Machine. Science. 2000;289(5488):2354-6. doi: 10.1126/science.289.5488.2354.
26. Bolon DN, Wah DA, Hersch GL, Baker TA, Sauer RT. Bivalent Tethering of SspB to ClpXP Is Required for Efficient Substrate Delivery: A Protein-Design Study. Mol Cell. 2004;13(3):443-9. doi: 10.1016/S1097-2765(04)00027-9.
27. Ghanbarpour A, Fei X, Baker TA, Davis JH, Sauer RT. The SspB adaptor drives structural changes in the AAA+ ClpXP protease during ssrA-tagged substrate delivery. Proc Natl Acad Sci U S A. 2023;120(6):e2219044120. doi: 10.1073/pnas.2219044120.
28. Gonzalez M, Rasulova F, Maurizi MR, Woodgate R. Subunit-specific degradation of the UmuD/D' heterodimer by the ClpXP protease: the role of *trans* recognition in UmuD' stability. EMBO J. 2000;19(19):5251-8. doi: 10.1093/emboj/19.19.5251.
29. Neher SB, Sauer RT, Baker TA. Distinct peptide signals in the UmuD and UmuD' subunits of UmuD/D' mediate tethering and substrate processing by the ClpXP protease. Proc Natl Acad Sci U S A. 2003;100(23):13219-24. doi: 10.1073/pnas.2235804100.
30. Zhou Y, Gottesman S, Hoskins JR, Maurizi MR, Wickner S. The RssB response regulator directly targets ς^S for degradation by ClpXP. Genes Dev. 2001;15(5):627-37. doi: 10.1101/gad.864401. PubMed PMID: 11238382; PubMed Central PMCID: PMCPMC312640.
31. Stüdemann A, Noirclerc-Savoye M, Klauck E, Becker G, Schneider D, Hengge R. Sequential recognition of two distinct sites in σ^S by the proteolytic targeting factor RssB and ClpX. EMBO J. 2003;22(16):4111-20. doi: 10.1093/emboj/cdg411.
32. Engman J, Rogstam A, Frees D, Ingmer H, Wachenfeldt Cv. The YjbH Adaptor Protein Enhances Proteolysis of the Transcriptional Regulator Spx in *Staphylococcus aureus*. J Bacteriol. 2012;194(5):1186-94. doi: 10.1128/jb.06414-11.
33. Panasenko OO, Bezrukov F, Komarynets O, Renzoni A. YjbH Solubility Controls Spx in *Staphylococcus aureus*: Implication for MazEF Toxin-Antitoxin System Regulation. Front

Microbiol. 2020;11:113. Epub 20200206. doi: 10.3389/fmicb.2020.00113. PubMed PMID: 32117138; PubMed Central PMCID: PMCPMC7016130.
34. Nielsen TK, Petersen IB, Xu L, Barbuti MD, Mebus V, Justh A, et al. The Spx stress regulator confers high-level β-lactam resistance and decreases susceptibility to last-line antibiotics in methicillin-resistant *Staphylococcus aureus*. Antimicrob Agents Chemother. 2024;68(6):e00335-24. doi: 10.1128/aac.00335-24.
35. Garg SK, Kommineni S, Henslee L, Zhang Y, Zuber P. The YjbH Protein of *Bacillus subtilis* Enhances ClpXP-Catalyzed Proteolysis of Spx. J Bacteriol. 2009;191(4):1268-77. doi: 10.1128/jb.01289-08.
36. Chan CM, Hahn E, Zuber P. Adaptor bypass mutations of *Bacillus subtilis* suggest a mechanism for YjbH-enhanced proteolysis of the regulator Spx by ClpXP. Mol Microbiol. 2014;93(3):426-38. doi: 10.1111/mmi.12671.
37. Pamp SJ, Frees D, Engelmann S, Hecker M, Ingmer H. Spx Is a Global Effector Impacting Stress Tolerance and Biofilm Formation in *Staphylococcus aureus*. J Bacteriol. 2006;188(13):4861-70. doi: doi:10.1128/jb.00194-06.
38. Feng J, Michalik S, Varming AN, Andersen JH, Albrecht D, Jelsbak L, et al. Trapping and Proteomic Identification of Cellular Substrates of the ClpP Protease in *Staphylococcus aureus*. J Proteome Res. 2013;12(2):547-58. doi: 10.1021/pr300394r.
39. Stahlhut SG, Alqarzaee AA, Jensen C, Fisker NS, Pereira AR, Pinho MG, et al. The ClpXP protease is dispensable for degradation of unfolded proteins in *Staphylococcus aureus*. Sci Rep. 2017;7(1):11739. doi: 10.1038/s41598-017-12122-y.
40. Bæk KT, Gründling A, Mogensen RG, Thøgersen L, Petersen A, Paulander W, et al. β-Lactam Resistance in Methicillin-Resistant *Staphylococcus aureus* USA300 Is Increased by Inactivation of the ClpXP Protease. Antimicrob Agents Chemother. 2014;58(8):4593-603. doi: 10.1128/aac.02802-14.
41. Jensen C, Bæk KT, Gallay C, Thalsø-Madsen I, Xu L, Jousselin A, et al. The ClpX chaperone controls autolytic splitting of *Staphylococcus aureus* daughter cells, but is bypassed by β-lactam antibiotics or inhibitors of WTA biosynthesis. PLoS Path. 2019;15(9):e1008044. doi: 10.1371/journal.ppat.1008044.
42. Bæk KT, Bowman L, Millership C, Søgaard MD, Kaever V, Siljamäki P, et al. The Cell Wall Polymer Lipoteichoic Acid Becomes Nonessential in *Staphylococcus aureus* Cells Lacking the ClpX Chaperone. mBio. 2016;7(4):10.1128/mbio.01228-16. doi: 10.1128/mbio.01228-16.
43. Henriksen C, Bæk KT, Wacnik K, Gallay C, Veening J-W, Foster SJ, et al. The ClpX chaperone and a hypermorphic FtsA variant with impaired self-interaction are mutually compensatory for coordinating *Staphylococcus aureus* cell division. Mol Microbiol. 2024;121(1):98-115. doi: 10.1111/mmi.15200.
44. Frees D, Qazi SNA, Hill PJ, Ingmer H. Alternative roles of ClpX and ClpP in *Staphylococcus aureus* stress tolerance and virulence. Mol Microbiol. 2003;48(6):1565-78. doi: 10.1046/j.1365-2958.2003.03524.x.
45. Jensen C, Fosberg MJ, Thalsø-Madsen I, Bæk KT, Frees D. *Staphylococcus aureus* ClpX localizes at the division septum and impacts transcription of genes involved in cell division, T7-secretion, and SaPI5-excision. Sci Rep. 2019;9(1):16456. doi: 10.1038/s41598-019-52823-0.
46. Bayles KW. The bactericidal action of penicillin: new clues to an unsolved mystery. Trends Microbiol. 2000;8(6):274-8. doi: 10.1016/S0966-842X(00)01762-5.
47. Schneider T, Sahl H-G. An oldie but a goodie – cell wall biosynthesis as antibiotic target pathway. Intl J Med Microbiol. 2010;300(2):161-9. doi: 10.1016/j.ijmm.2009.10.005.
48. Lock RL, Harry EJ. Cell-division inhibitors: new insights for future antibiotics. Nat Rev Drug Discov. 2008;7(4):324-38. doi: 10.1038/nrd2510.
49. Tipper DJ, Strominger JL. Mechanism of action of penicillins: a proposal based on their structural similarity to acyl-D-alanyl-D-alanine. Proc Natl Acad Sci U S A. 1965;54(4):1133-41. doi: 10.1073/pnas.54.4.1133.

50. Tomasz A, Waks S. Mechanism of action of penicillin: triggering of the pneumococcal autolytic enzyme by inhibitors of cell wall synthesis. Proc Natl Acad Sci U S A. 1975;72(10):4162-6. doi: 10.1073/pnas.72.10.4162.
51. Kitano K, Tomasz A. Triggering of autolytic cell wall degradation in *Escherichia coli* by beta-lactam antibiotics. Antimicrob Agents Chemother. 1979;16(6):838-48. doi: 10.1128/aac.16.6.838.
52. Rogers HJ, Forsberg CW. Role of Autolysins in the Killing of Bacteria by Some Bactericidal Antibiotics. J Bacteriol. 1971;108(3):1235-43. doi: 10.1128/jb.108.3.1235-1243.1971.
53. Giesbrecht P, Kersten T, Maidhof H, Wecke J. Staphylococcal Cell Wall: Morphogenesis and Fatal Variations in the Presence of Penicillin. Microbiol Mol Biol Rev. 1998;62(4):1371-414. doi: 10.1128/mmbr.62.4.1371-1414.1998.
54. Lorian V. Some Effects of Subinhibitory Concentrations of Penicillin on the Structure and Division of Staphylococci. Antimicrob Agents Chemother. 1975;7(6):864-70. doi: 10.1128/aac.7.6.864.
55. Antignac A, Sieradzki K, Tomasz A. Perturbation of Cell Wall Synthesis Suppresses Autolysis in *Staphylococcus aureus*: Evidence for Coregulation of Cell Wall Synthetic and Hydrolytic Enzymes. J Bacteriol. 2007;189(21):7573-80. doi: 10.1128/jb.01048-07.
56. Pereira SFF, Henriques AO, Pinho MG, De Lencastre H, Tomasz A. Evidence for a dual role of PBP1 in the cell division and cell separation of *Staphylococcus aureus*. Mol Microbiol. 2009;72(4):895-904. doi: 10.1111/j.1365-2958.2009.06687.x.
57. Tomasz A, Albino A, Zanati EVE. Multiple Antibiotic Resistance in a Bacterium with Suppressed Autolytic System. Nature. 1970;227(5254):138-40. doi: 10.1038/227138a0.
58. de Bakker V, Liu X, Bravo AM, Veening J-W. CRISPRi-seq for genome-wide fitness quantification in bacteria. Nat Protoc. 2022;17(2):252-81. doi: 10.1038/s41596-021-00639-6.
59. Liu X, Bakker Vd, Heggenhougen MV, Mårli MT, Frøynes AH, Salehian Z, et al. Genome-wide CRISPRi screens for high-throughput fitness quantification and identification of determinants for dalbavancin susceptibility in *Staphylococcus aureus*. mSystems. 2024;9(7):e01289-23. doi: 10.1128/msystems.01289-23.
60. Mårli MT, Nordraak AOO, de Bakker V, Winther AR, Liu X, Veening J-W, et al. Genome-wide analysis of fitness determinants of *Staphylococcus aureus* during growth in milk. bioRxiv. 2024:2024.10.31.621336. doi: 10.1101/2024.10.31.621336.
61. Zimmermann L, Stephens A, Nam S-Z, Rau D, Kübler J, Lozajic M, et al. A completely reimplemented MPI bioinformatics toolkit with a new HHpred server at its core. J Mol Biol. 2018;430(15):2237-43. doi: 10.1016/j.jmb.2017.12.007.
62. Finn RD, Clements J, Eddy SR. HMMER web server: interactive sequence similarity searching. Nucleic Acids Res. 2011;39(suppl_2):W29-W37. doi: 10.1093/nar/gkr367.
63. !!! INVALID CITATION !!! [63-65].
64. Allan RK, Ratajczak T. Versatile TPR domains accommodate different modes of target protein recognition and function. Cell Stress and Chaperones. 2011;16(4):353-67. doi: 10.1007/s12192-010-0248-0.
65. D'Andrea LD, Regan L. TPR proteins: the versatile helix. Trends Biochem Sci. 2003;28(12):655-62. doi: 10.1016/j.tibs.2003.10.007.
66. Blatch GL, Lässle M. The tetratricopeptide repeat: a structural motif mediating protein-protein interactions. BioEssays. 1999;21(11):932-9. doi: 10.1002/(SICI)1521-1878(199911)21:11<932::AID-BIES5>3.0.CO;2-N.
67. Perez-Riba A, Itzhaki LS. The tetratricopeptide-repeat motif is a versatile platform that enables diverse modes of molecular recognition. Curr Opin Struct Biol. 2019;54:43-9. doi: 10.1016/j.sbi.2018.12.004.
68. Oliveira Paiva AM, Friggen AH, Qin L, Douwes R, Dame RT, Smits WK. The Bacterial Chromatin Protein HupA Can Remodel DNA and Associates with the Nucleoid in *Clostridium difficile*. J Mol Biology. 2019;431(4):653-72. doi: 10.1016/j.jmb.2019.01.001.

69. Eckler SA, Kuehn R, Gautam M. Deletion of N-terminal rapsyn domains disrupts clustering and has dominant negative effects on clustering of full-length rapsyn. Neuroscience. 2005;131(3):661-70. doi: 10.1016/j.neuroscience.2004.11.035.
70. Krachler AM, Sharma A, Kleanthous C. Self-association of TPR domains: Lessons learned from a designed, consensus-based TPR oligomer. Proteins. 2010;78(9):2131-43. doi: 10.1002/prot.22726.
71. McCallum N, Spehar G, Bischoff M, Berger-Bächi B. Strain dependence of the cell wall-damage induced stimulon in *Staphylococcus aureus*. Biochimi Biophys Acta. 2006;1760(10):1475-81. doi: 10.1016/j.bbagen.2006.06.008.
72. Boyle-Vavra S, Yin S, Jo DS, Montgomery CP, Daum RS. VraT/YvqF is required for methicillin resistance and activation of the VraSR regulon in *Staphylococcus aureus*. Antimicrob Agents Chemother. 2013;57(1):83-95. doi: 10.1128/aac.01651-12.
73. Saß P. Antibacterial treatment of *Staphylococcus aureus*: Response and resistance to the lantibiotic mersacidin and evaluation of endolysins as a biofilm treatment strategy. Bonn: University of Bonn; 2009.
74. Mensa B, Howell GL, Scott R, DeGrado WF. Comparative Mechanistic Studies of Brilacidin, Daptomycin, and the Antimicrobial Peptide LL16. Antimicrob Agents Chemother. 2014;58(9):5136-45. doi: 10.1128/aac.02955-14.
75. Le TNB. Studying on protein stress response in *Staphylococcus aureus*. Greifswald University of Greifswald; 2008.
76. Kuroda M, Kuroda H, Oshima T, Takeuchi F, Mori H, Hiramatsu K. Two-component system VraSR positively modulates the regulation of cell-wall biosynthesis pathway in *Staphylococcus aureus*. Mol Microbiol. 2003;49(3):807-21. doi: 10.1046/j.1365-2958.2003.03599.x.
77. Chan YGY, Frankel MB, Missiakas D, Schneewind O. SagB Glucosaminidase Is a Determinant of *Staphylococcus aureus* Glycan Chain Length, Antibiotic Susceptibility, and Protein Secretion. J Bacteriol. 2016;198(7):1123-36. doi: 10.1128/jb.00983-15.
78. Campbell J, Singh AK, Santa Maria JP, Jr., Kim Y, Brown S, Swoboda JG, et al. Synthetic Lethal Compound Combinations Reveal a Fundamental Connection between Wall Teichoic Acid and Peptidoglycan Biosyntheses in *Staphylococcus aureus*. ACS Chem Biol. 2011;6(1):106-16. doi: 10.1021/cb100269f.
79. Campbell J, Singh AK, Swoboda JG, Gilmore MS, Wilkinson BJ, Walker S. An Antibiotic That Inhibits a Late Step in Wall Teichoic Acid Biosynthesis Induces the Cell Wall Stress Stimulon in *Staphylococcus aureus*. Antimicrob Agents Chemother. 2012;56(4):1810-20. doi: doi:10.1128/aac.05938-11.
80. Löfblom J, Kronqvist N, Uhlén M, Ståhl S, Wernérus H. Optimization of electroporation-mediated transformation: *Staphylococcus carnosus* as model organism. Journal of Applied Microbiology. 2007;102(3):736-47. doi: 10.1111/j.1365-2672.2006.03127.x.
81. Stamsås GA, Myrbråten IS, Straume D, Salehian Z, Veening J-W, Håvarstein LS, et al. CozEa and CozEb play overlapping and essential roles in controlling cell division in *Staphylococcus aureus*. Mol Microbiol. 2018;109(5):615-32. doi: 10.1111/mmi.13999.
82. Myrbråten IS, Stamsås GA, Chan H, Angeles DM, Knutsen TM, Salehian Z, et al. SmdA is a Novel Cell Morphology Determinant in *Staphylococcus aureus*. mBio. 2022;13(2):e03404-21. doi: 10.1128/mbio.03404-21.
83. Arnaud M, Chastanet A, Debarbouille M. New vector for efficient allelic replacement in naturally nontransformable, low-GC-content, Gram-positive bacteria. Appl Environ Microbiol. 2004;70(11):6887-91. doi: 10.1128/AEM.70.11.6887-6891.2004. PubMed PMID: 15528558; PubMed Central PMCID: PMCPMC525206.
84. Arnaud M, Chastanet A, Débarbouillé M. New Vector for Efficient Allelic Replacement in Naturally Nontransformable, Low-GC-Content, Gram-Positive Bacteria. Appl Environ Microbiol. 2004;70(11):6887-91. doi: 10.1128/AEM.70.11.6887-6891.2004.

85. Kearse M, Moir R, Wilson A, Stones-Havas S, Cheung M, Sturrock S, et al. Geneious Basic: An integrated and extendable desktop software platform for the organization and analysis of sequence data. Bioinformatics. 2012;28(12):1647-9. doi: 10.1093/bioinformatics/bts199.
86. Ducret A, Quardokus EM, Brun YV. MicrobeJ, a tool for high throughput bacterial cell detection and quantitative analysis. Nat Microbiol. 2016;1(7):16077. doi: 10.1038/nmicrobiol.2016.77.
87. Barbuti MD, Lambert E, Myrbråten IS, Ducret A, Stamsås GA, Wilhelm L, et al. The function of CozE proteins is linked to lipoteichoic acid biosynthesis in *Staphylococcus aureus*. mBio. 2024;15(6):e01157-24. doi: 10.1128/mbio.01157-24.
88. Teufel F, Almagro Armenteros JJ, Johansen AR, Gislason MH, Pihl SI, Tsirigos KD, et al. SignalP 6.0 predicts all five types of signal peptides using protein language models. Nat Biotechnol. 2022;40(7):1023-5. Epub 20220103. doi: 10.1038/s41587-021-01156-3. PubMed PMID: 34980915; PubMed Central PMCID: PMCPMC9287161.
89. Hallgren J, Tsirigos KD, Pedersen MD, Almagro Armenteros JJ, Marcatili P, Nielsen H, et al. DeepTMHMM predicts alpha and beta transmembrane proteins using deep neural networks. bioRxiv. 2022:2022.04.08.487609. doi: 10.1101/2022.04.08.487609.
90. Altschul SF, Gish W, Miller W, Myers EW, Lipman DJ. Basic local alignment search tool. J Mol Biol. 1990;215(3):403-10. doi: 10.1016/S0022-2836(05)80360-2. PubMed PMID: 2231712.
91. Sievers F, Wilm A, Dineen D, Gibson TJ, Karplus K, Li W, et al. Fast, scalable generation of high-quality protein multiple sequence alignments using Clustal Omega. Mol Syst Biol. 2011;7:539. Epub 20111011. doi: 10.1038/msb.2011.75. PubMed PMID: 21988835; PubMed Central PMCID: PMCPMC3261699.
92. Waterhouse AM, Procter JB, Martin DM, Clamp M, Barton GJ. Jalview Version 2--a multiple sequence alignment editor and analysis workbench. Bioinformatics. 2009;25(9):1189-91. Epub 20090116. doi: 10.1093/bioinformatics/btp033. PubMed PMID: 19151095; PubMed Central PMCID: PMCPMC2672624.
93. Tamura K, Stecher G, Kumar S. MEGA11: Molecular Evolutionary Genetics Analysis Version 11. Mol Biol Evol. 2021;38(7):3022-7. doi: 10.1093/molbev/msab120. PubMed PMID: 33892491; PubMed Central PMCID: PMCPMC8233496.
94. Karpenahalli MR, Lupas AN, Soding J. TPRpred: a tool for prediction of TPR-, PPR- and SEL1-like repeats from protein sequences. BMC Bioinformatics. 2007;8:2. Epub 20070103. doi: 10.1186/1471-2105-8-2. PubMed PMID: 17199898; PubMed Central PMCID: PMCPMC1774580.
95. Abramson J, Adler J, Dunger J, Evans R, Green T, Pritzel A, et al. Accurate structure prediction of biomolecular interactions with AlphaFold 3. Nature. 2024;630(8016):493-500. doi: 10.1038/s41586-024-07487-w.
96. Meng EC, Goddard TD, Pettersen EF, Couch GS, Pearson ZJ, Morris JH, et al. UCSF ChimeraX: Tools for structure building and analysis. Protein Sci. 2023;32(11):e4792. doi: 10.1002/pro.4792.
97. Schrodinger, LLC. The PyMOL Molecular Graphics System, Version 1.8. 2015.

1034 **Figures**

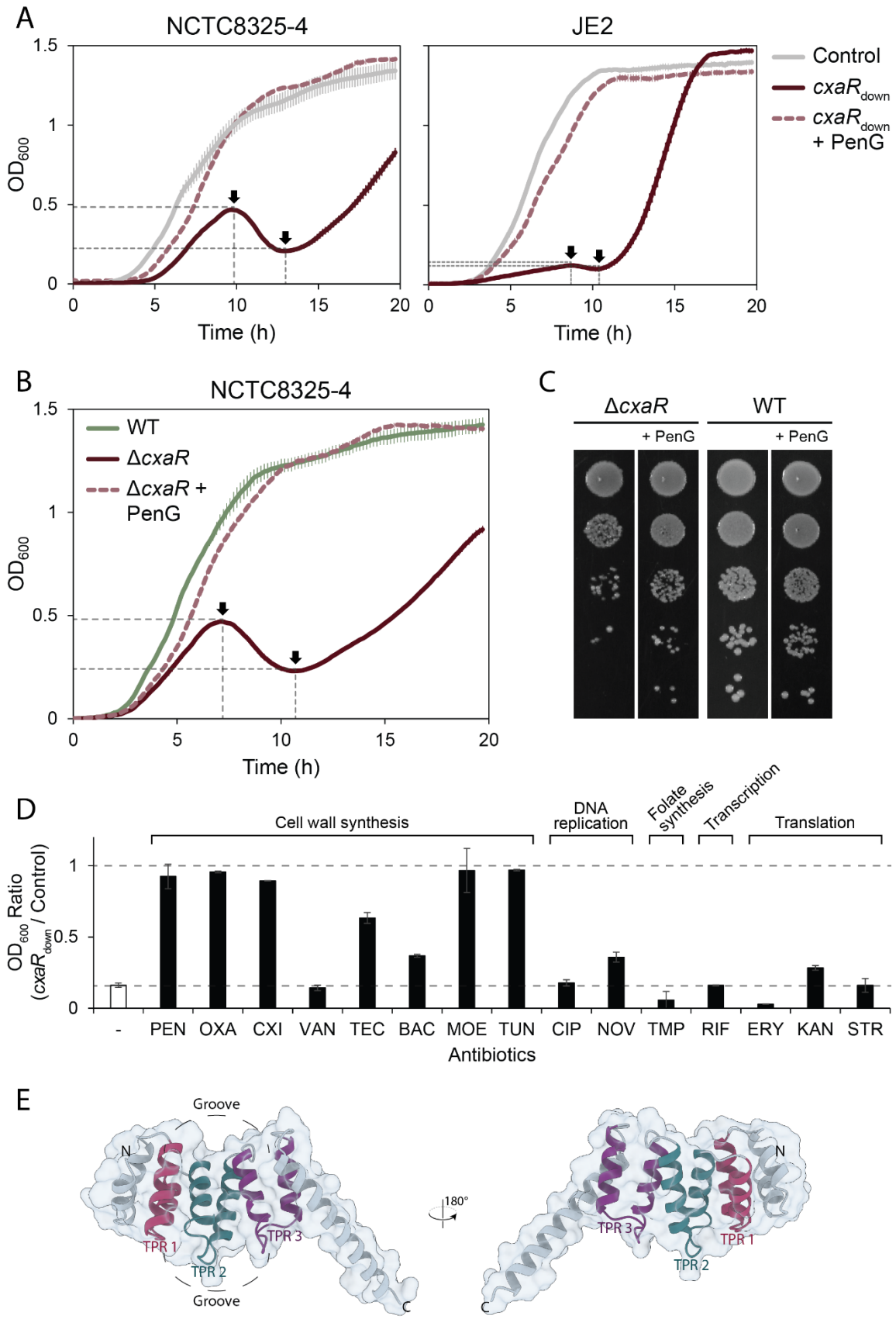

1035
1036 **Fig. 1. Lack of CxaR leads to a biphasic growth defect that can be rescued by sublethal**
1037 **concentrations of various antibiotics.**

1038 (**A**) Growth curves of the *cxaR* knockdown mutants (*cxaR*$_{down}$) and CRISPRi control strains in TSB at
1039 37°C for both NCTC8325-4 and JE2. Gene knockdown was induced with addition of 500 µM IPTG, and
1040 growth of the *cxaR*$_{down}$ mutants was restored with addition of penicillin G (1 ng/mL for NCTC8325-4 and
1041 5 ng/mL for JE2). The graphs represent averages with standard deviation from triplicate measurements.

1042 (**B**) Growth curves of the NCTC8325-4 *cxaR* deletion mutant and wild-type in TSB at 37°C. Growth of
1043 the Δ*cxaR* mutant was restored with addition of penicillin G (1 ng/mL). The graphs represent averages
1044 with standard deviation from triplicate measurements.

1045 (**C**) Growth of the NCTC8325-4 *cxaR* deletion mutant and wild-type on TSA with or without penicillin G
1046 (1 ng/mL) after 10 hours of incubation at 37°C. The bacterial cultures were sampled after 10 hours of
1047 incubation in TSB (± penicillin G) and 10-fold dilution series were spotted onto TSA plates (± penicillin
1048 G).

1049 (**D**) Relative growth of the JE2 *cxaR*$_{down}$ mutant compared to the CRISPRi control after 8 hours of
1050 incubation at 37°C in the presence or absence of MIC_1 concentrations of various antibiotics. Data
1051 represent the average growth ratio ± standard deviation from the mean of two biological replicates for
1052 the antibiotic-treated samples, and from 30 biological replicates for the untreated control. A ratio of 1
1053 indicates that the two strains have reached the exact same OD_{600} after 8 hours of incubation. In the
1054 absence of antibiotics, the ratio was approximately 0.16. Notably, several of the antibiotics stimulated
1055 growth of the *cxaR*$_{down}$ mutant, leading to a significant increase in the growth ratio. For the individual
1056 growth of the *cxaR*$_{down}$ and CRISPRi control strain with increasing concentrations of the various
1057 antibiotics, see **Fig. S3**.

1058 (**E**) The AlphaFold 3-predicted structure of CxaR, with its three proposed anti-parallel sets of TPR-like
1059 helices colored red, blue, and purple. These helices form a slightly concave surface groove, as indicated
1060 in the figure

1061

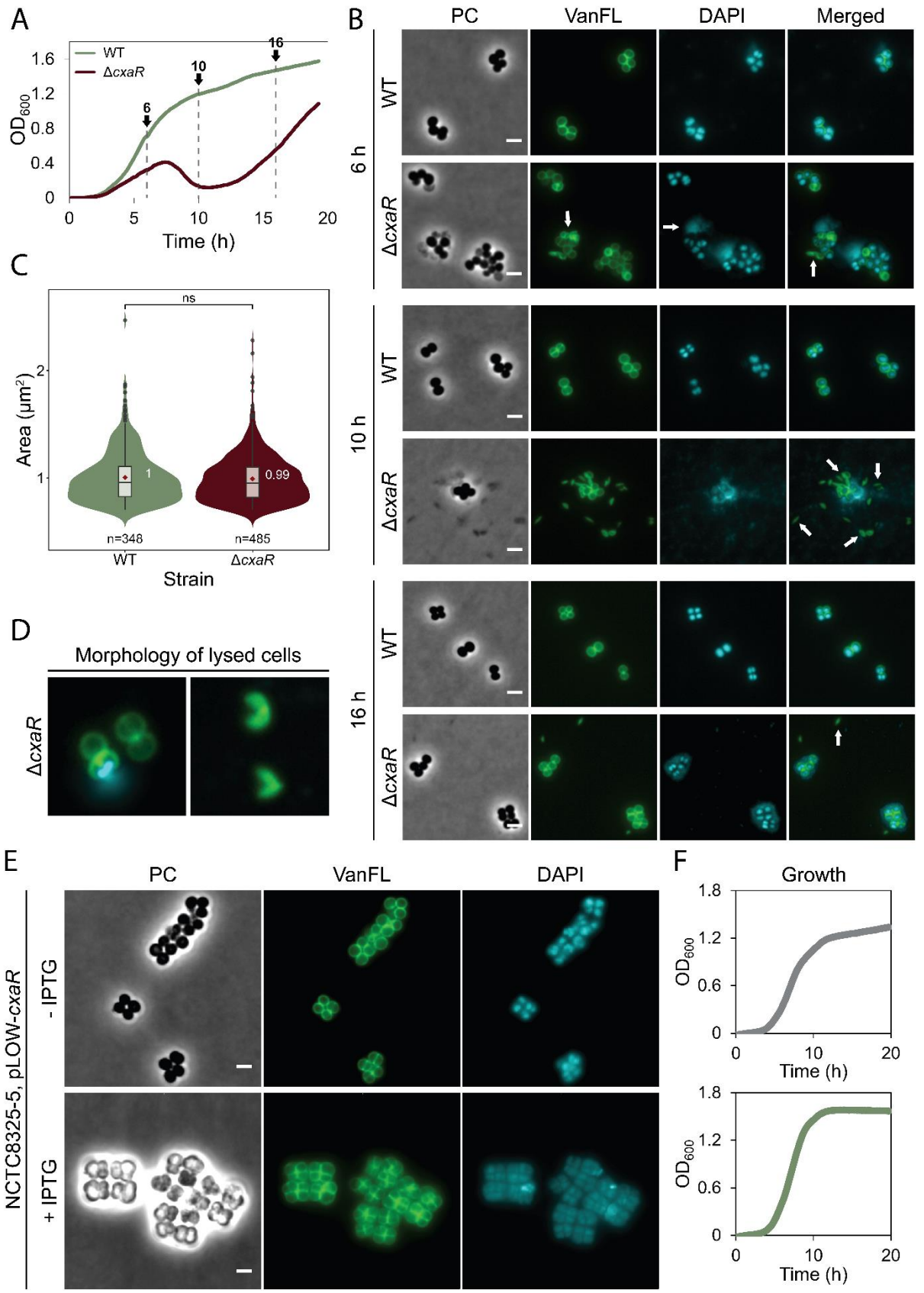

Fig. 2. *cxaR* deletion increases lytic activity, while overexpression impairs cell division.

(**A**) Growth curves of NCTC8325-4 Δ*cxaR* and wild-type, with the timepoints for cell sampling used in microscopy (shown in panel **B**). The graphs represent averages from triplicate measurements.

1066 (**B**) Representative phase-contrast and fluorescence micrographs of Δ*cxaR* and wild-type cells stained
1067 with VanFL (cell wall) and DAPI (nucleoid) after 6, 10, and 16 hours of incubation at 37°C. White arrows
1068 point to cells with peptidoglycan hydrolysis (VanFL), nucleoid dispersal (DAPI), and anucleate cells
1069 (merged). The scale bars are 2 µm.

1070 (**C**) Violin plots showing the cell area distributions (in μm^2) for wild-type (1.00 ± 0.24 μm^2) and Δ*cxaR*
1071 (0.99 ± 0.22 μm^2) after 6 hours at 37°C, determined using MicrobeJ. No significant difference in size
1072 was detected between the strains (ns, *P*-value > 0.05, Mann-Whitney U test). The number of cells
1073 analyzed is indicated in the figure.

1074 (**D**) Magnified merged fluorescence images showing the predominant lytic phenotypes of the Δ*cxaR*
1075 cells. Cells commonly exhibited a nick at septum accompanied by DNA dispersal at the earlier
1076 timepoints, progressing to crescent-shaped debris by the 10-hour mark, indicative of widespread lysis.

1077 (**E**) Representative phase-contrast and fluorescence micrographs of NCTC8325-4 cells carrying the
1078 pLOW-*cxaR* plasmid for inducible overexpression of CxaR, stained with VanFL (cell wall) and DAPI
1079 (nucleoid). Cells were grown at 37°C with or without 500 µM IPTG until an OD_{600} of approximately 0.4
1080 was reached. Upon induction, cells displayed clear separation defects, including cell clumping and
1081 enlarged cells with multiple septa. The scale bars are 2 µm.

1082 (**F**) Growth curves of NCTC8325-4 cells with the pLOW-*cxaR* plasmid, grown in the absence (gray) or
1083 presence (green) of 500 µM IPTG for CxaR overexpression. The graphs represent averages from
1084 triplicate measurements.

1085

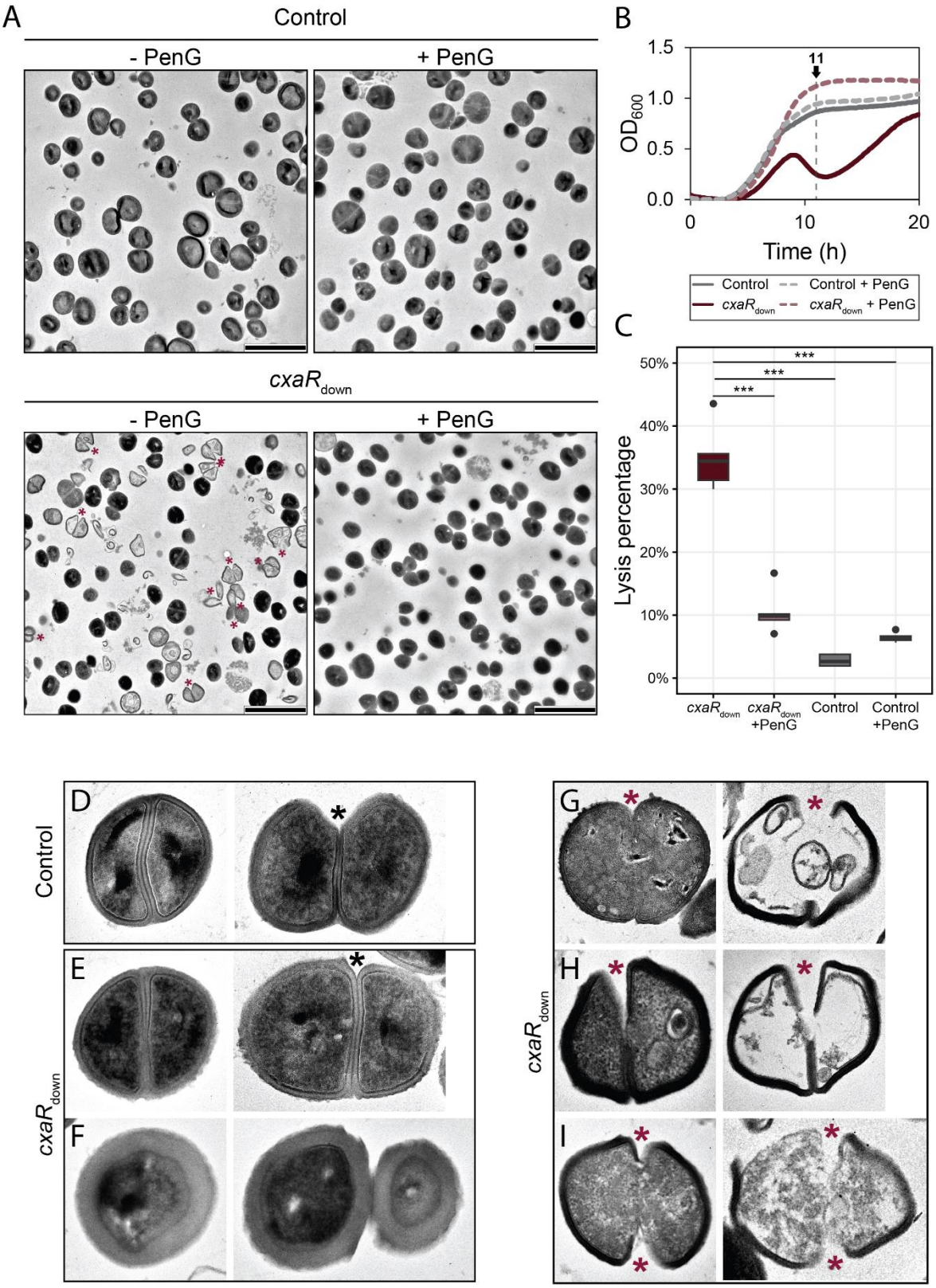

Fig. 3. The increased lysis observed in the absence of CxaR is due to premature splitting of daughter cells, a phenomenon significantly mitigated by penicillin G treatment.

(**A**) TEM images of the NCTC8325-4 *cxaR* knockdown mutant (*cxaR*$_{down}$) and CRISPRi control strain grown in TSB for 11 hours at 37°C, in the absence or presence of sublethal concentrations of penicillin G (1 ng/mL). Red asterisks mark cells that have undergone cell splitting prior to septum completion. The scale bars are 2 µm.

1093 (**B**) Growth curves of NCTC8325-4 *cxaR*$_{down}$ and CRISPRi control, with (dashed line) or without (solid
1094 line) sublethal concentrations of penicillin G (1 ng/mL), showing the sampling timepoint for TEM imaging.
1095 The graphs represent averages from triplicate measurements.

1096 (**C**) Box plots showing the proportion of lysed cells, as observed by TEM, that retained minimal structural
1097 integrity. Significant differences between the strains are indicated with asterisks (***, *P*-value < 0.0005,
1098 Tukey's Honest Significant Difference test). The number of cells analyzed, from left to right, is 231, 303,
1099 241, and 250.

1100 (**D-I**) Representative TEM images of CRISPRi control and *cxaR*$_{down}$ cells, highlighting their characteristic
1101 morphologies. (**D**) Control cells displaying normal coccoid morphology. *cxaR* knockdown cells
1102 displaying: (**E**) wild-type-like morphology, (**F**) significantly thicker cell wall, (**G**) a septal nick prior to or at
1103 early stages of septal growth, (**H**) premature daughter cell splitting occurring just before septum
1104 completion, and (**I**) simultaneous splitting at both ends of the forming septum. Black asterisks mark cells
1105 in which hydrolysis of the peripheral septal wall occurred after septum completion, while red asterisks
1106 mark cells initiating daughter cell separation, despite an incomplete septum.

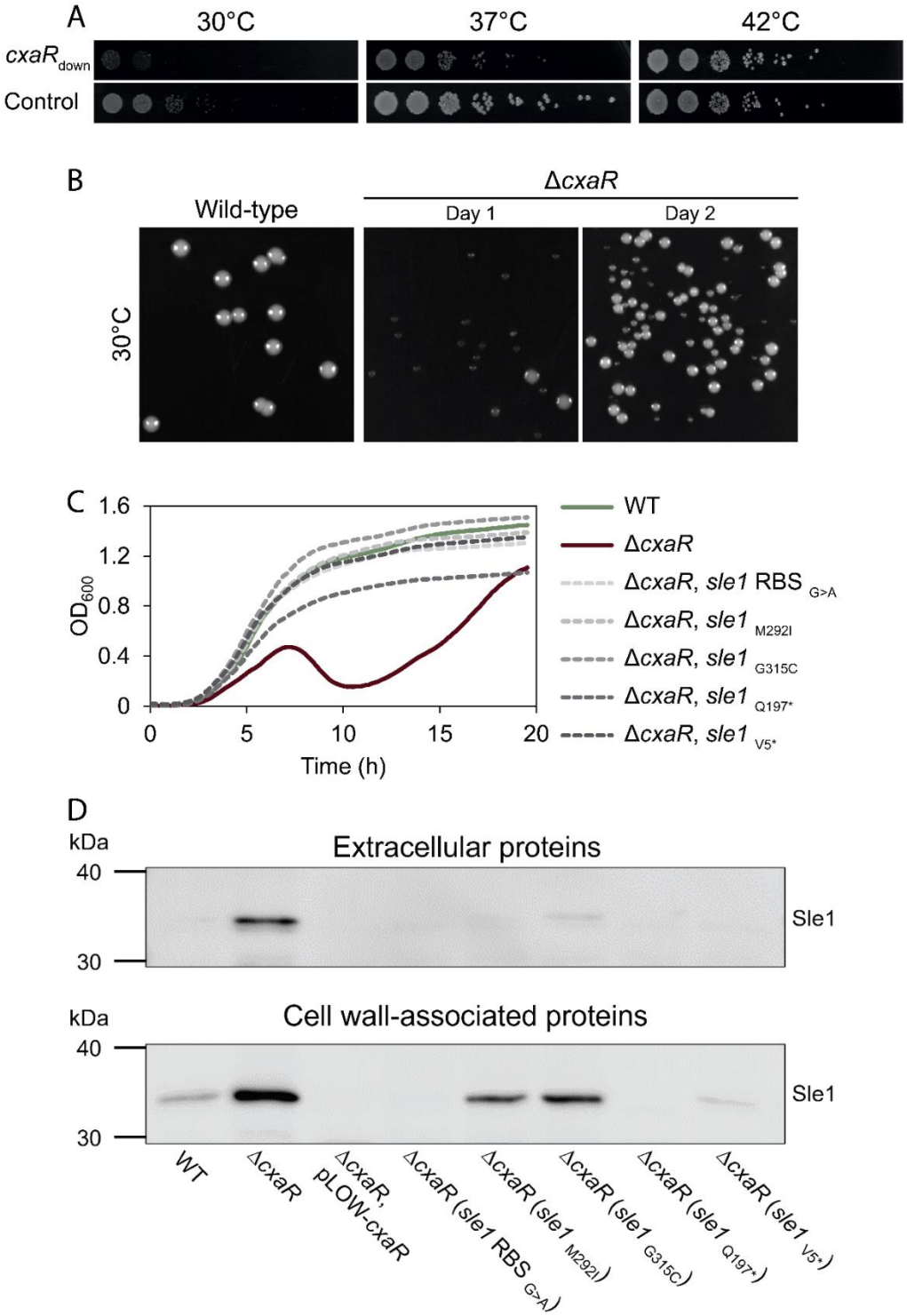

Fig. 4. Spontaneous *sle1*-associated mutations frequently rescued the defects of the *cxaR* deletion mutant at 30°C.

(**A**) Spotting assays comparing growth of the NCTC8325-4 *cxaR* knockdown mutant (*cxaR*$_{down}$) and CRISPRi control at 30°C, 37°C, and 42°C. The bacterial cultures were grown at 37°C to an OD_{600} of 0.5, 10-fold serially diluted, and 5 µL of each dilution was spotted onto TSA plates that were incubated at the indicated temperatures. Compared to the control, the *cxaR*$_{down}$ mutant was cold-sensitive and heat-stable.

1115 (**B**) At 30°C, the NCTC8325-4 Δ*cxaR* mutant formed both very small colonies and larger suppressor
1116 colonies, unlike the homogeneous colony size observed for wild-type. When overnight cultures of Δ*cxaR*
1117 grown at 37°C were plated on TSA and incubated at 30°C, some larger colonies appeared among the
1118 very small ones (day 1). When single colonies from these plates were grown overnight at 30°C and
1119 replated on TSA at 30°C, the plates exhibited predominantly large suppressor colonies (day 2).

1120 (**C**) Growth of five independently isolated large Δ*cxaR* colonies, all found to have different *sle1*-
1121 associated mutations, in TSB at 37°C. All five suppressor mutants displayed growth patterns more
1122 closely resembling the wild-type than the original Δ*cxaR* strain. The graphs represent averages from
1123 triplicate measurements.

1124 **(D)** Western blot analysis of Sle1 levels in the extracellular and cell wall-associated protein fractions of
1125 the Δ*cxaR* suppressors with *sle1*-associated mutations. The Sle1 levels of the suppressor mutants were
1126 compared to those of wild-type, *cxaR* deletion, and *cxaR* overexpressing cells.

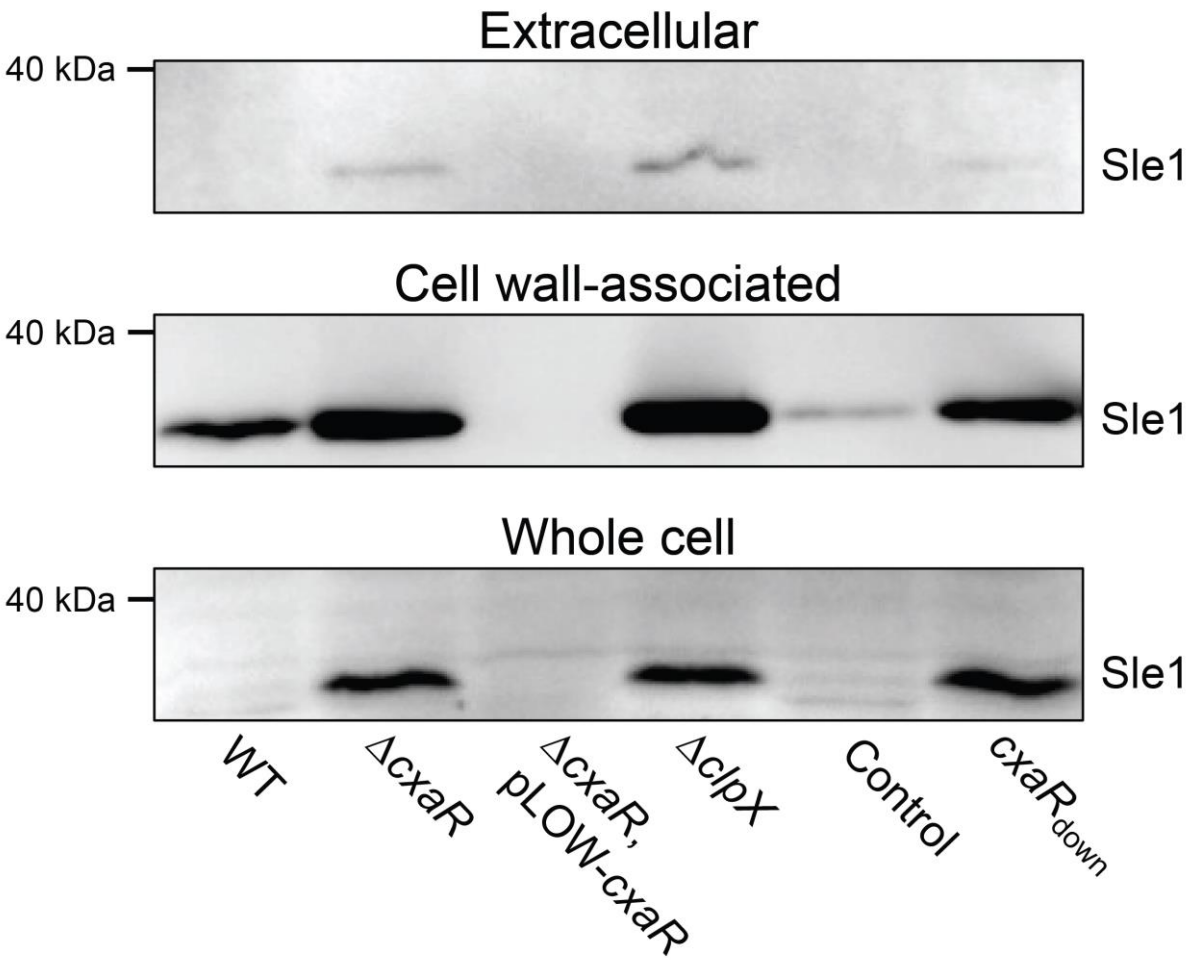

Fig. 5. Sle1 accumulates in the absence of CxaR, while overexpression of CxaR causes Sle1 depletion below detectable levels.

Western blot analysis of Sle1 levels in cell wall-associated protein fractions, extracellular protein fractions, and whole-cell lysates using an anti-Sle1 antibody. The blots show that Sle1 levels were elevated in NCTC8325-4 cells lacking CxaR (Δ*cxaR* and $cxaR_{down}$) or ClpX (Δ*clpX*), while Sle1 was depleted in NCTC8325-4 cells overexpressing CxaR (Δ*cxaR*, pLOW-*cxaR*), compared to the wild-type and CRISPRi control cells.

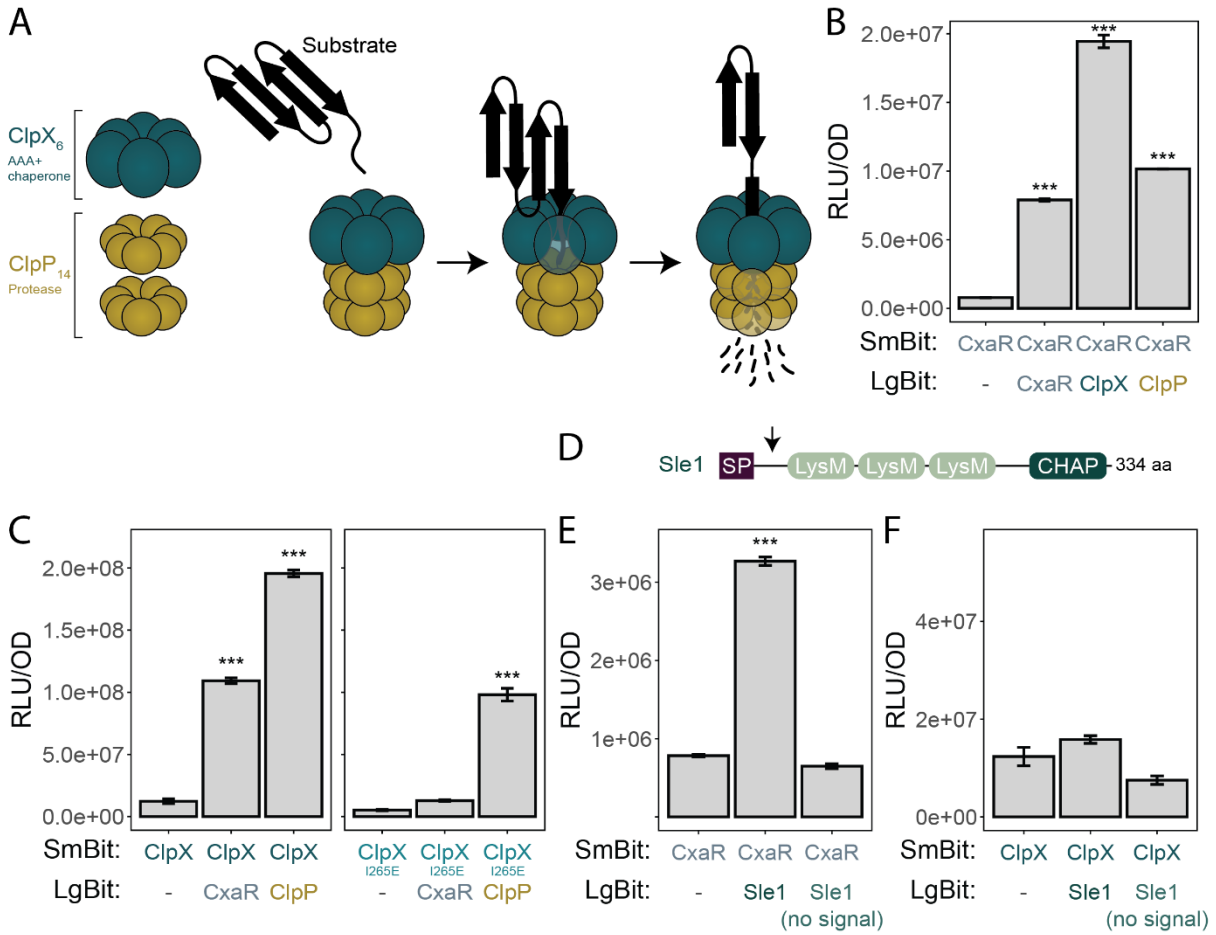

Fig. 6. CxaR interacts with ClpX and Sle1.

(**A**) Schematic overview of a single-capped ClpXP structure and its function. Single-capped ClpXP consist of a hexameric ClpX ATPase ring and two heptameric rings of the ClpP peptidase, forming a proteolytic complex. ClpX recognizes and unfolds protein substrates, either directly or via adaptor proteins, and translocates them through its central pore into the proteolytic chamber of ClpP, where they are degraded into small peptide fragments, ensuring selective and irreversible degradation of proteins in the cell.

(**B-C**) Split luciferase assays identifying potential protein-protein interactions between (**B**) CxaR and CxaR/ClpX/ClpP, and (**C**) ClpX/ClpX$_{I265E}$ and CxaR/ClpP. Bars represent mean luminescence (RLU/OD$_{600}$) from four replicates, with error bars indicating the standard deviation. Significant interactions were assessed with one-way ANOVA followed by Tukey's Honest Significant Difference test (***, *P*-value < 0.001). CxaR displayed self-interaction and interactions with both ClpX and ClpP. Similarly, ClpX interacted with CxaR and ClpP, however the interaction with CxaR appears to be lost when ClpX does not form a complex with ClpP.

(**D**) The modular structure of the Sle1 amidase, consisting of a N-terminal signal peptide (SP) for secretion, three cell wall-binding LysM domains, and an enzymatically active histidine-dependent amidohydrolase/peptidase (CHAP) C-terminal domain. The signal peptide of Sle1 is post-translationally processed, as indicated by the arrow.

(**E-F**) Split luciferase assays assessing potential protein-protein interactions between (**D**) CxaR and Sle1 (with and without the signal peptide), and (**E**) ClpX and Sle1 (with and without the signal peptide). Bars represent mean luminescence (RLU/OD$_{600}$) from four replicates, with error bars indicating the standard deviation. Significant interactions were assessed with one-way ANOVA followed by Tukey's Honest

1159 Significant Difference test (***, *P*-value < 0.001). CxaR showed interaction with the precursor of Sle1
1160 (with signal peptide), while ClpX did not interact with the precursor nor the mature form of Sle1.

1161

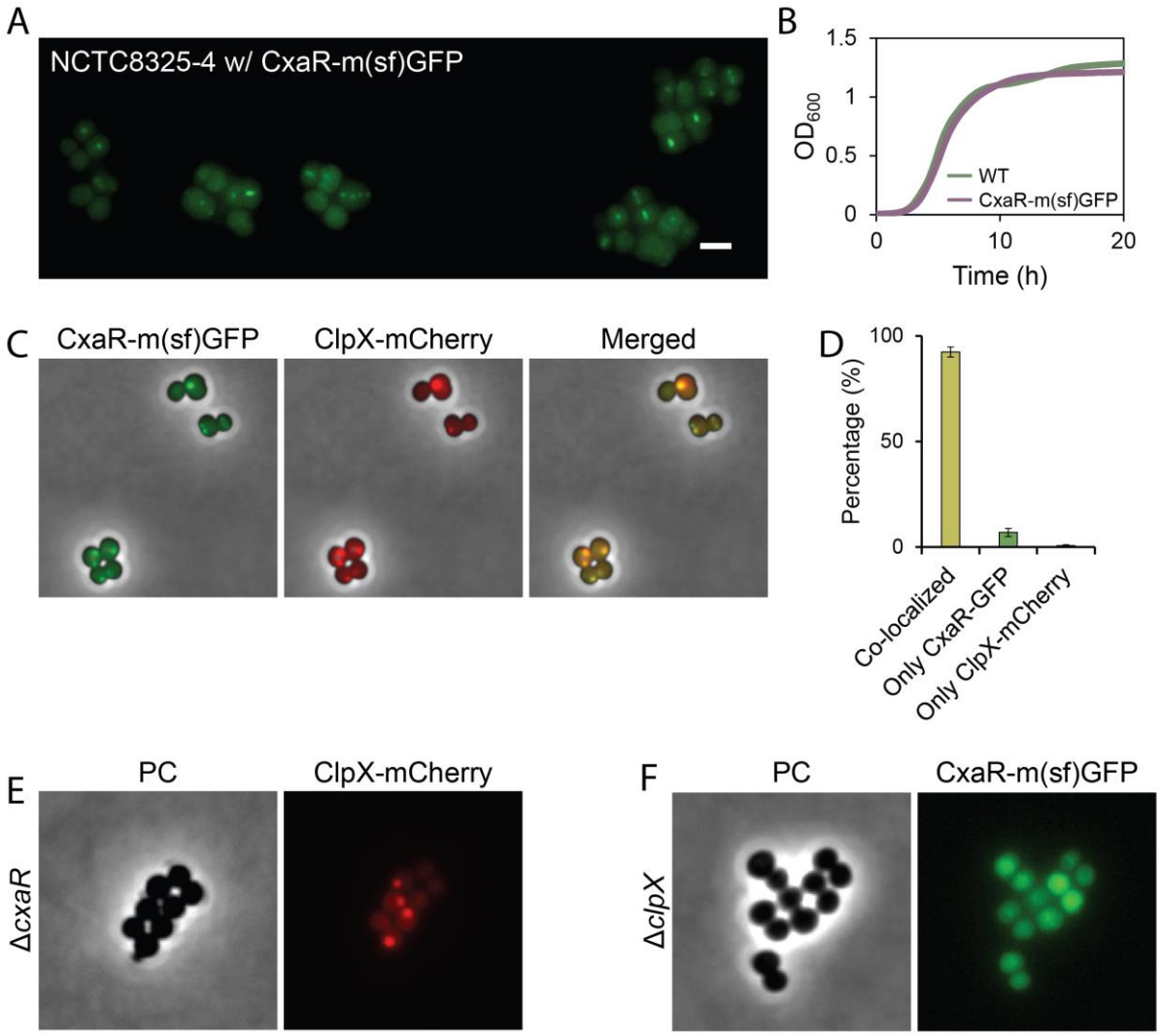

Fig. 7. CxaR localizes adjacent to the septum in a ClpX-dependent manner.

(**A**) Fluorescence microscopy of the NCTC8325-4 strain expressing chromosomally integrated CxaR-GFP under its native promoter, showing that CxaR-GFP localizes at midcell in dividing cells. The scale bar represents 2 µm.

(**B**) Growth curves of NCTC8325-4 wild-type and chromosomally expressing CxaR-GFP cells in TSB at 37°C, demonstrating that GFP tagging of CxaR does not impair growth. The graphs represent averages from triplicate measurements.

(**C**) Fluorescent microscopy of NCTC8325-4 cells co-expressing CxaR-GFP (from the chromosome) and ClpX-mCherry (from a plasmid induced with 80 µM IPTG), showing clear co-localization of the two proteins.

(**D**) Quantification of CxaR-GFP and ClpX-mCherry co-localization in NCTC8325-4 cells expressing both fusion proteins. Co-localization was analyzed by manual examination of the fluorescence signals in 300–350 randomly selected cells from two biological replicates (n = 635). CxaR-GFP and ClpX-mCherry were co-localized in 92.4 ± 2.4% of cells, 6.9 ± 1.9% of cells displayed only CxaR-GFP signal, and 0.6 ± 0.5% showed only ClpX-mCherry, confirming spatiotemporal co-localization of the two proteins during cell division.

(E-F) Fluorescence microscopy of (**H**) Δ*clpX* cells expressing CxaR-GFP from a plasmid and (**I**) Δ*cxaR* cells expressing ClpX-mCherry from a plasmid. Expression of the plasmids were induced with the addition of 10 µM and 160 uM IPTG, respectively. In the absence of ClpX, CxaR-GFP loses septal-

1182 adjacent localization, indicating that CxaR requires ClpX for its spatiotemporal localization. In contrast,
1183 ClpX-mCherry retained its focal localization pattern in Δ*cxaR* cells, demonstrating that ClpX
1184 localization does not depend on the presence of CxaR.

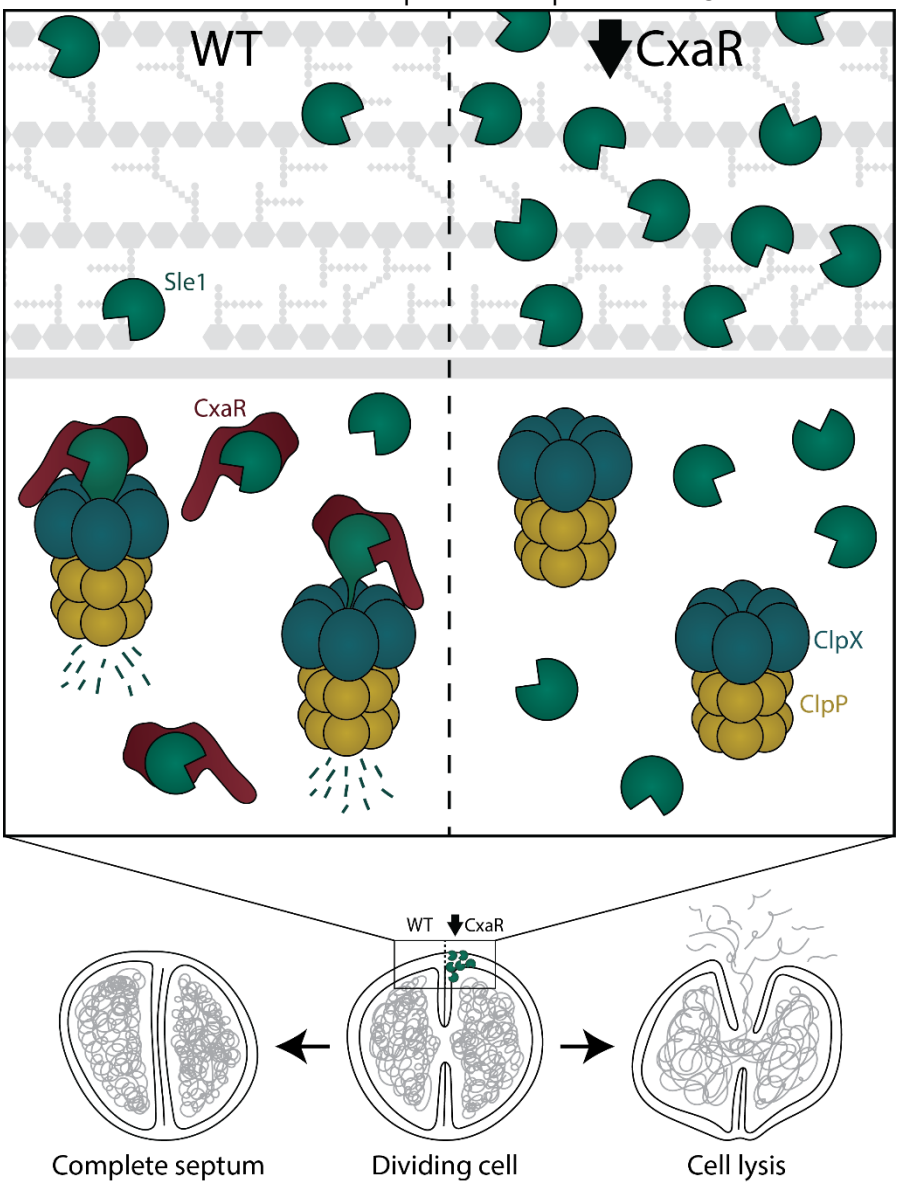

1185

1186 **Fig. 8. CxaR facilitates ClpXP-mediated degradation of Sle1, ensuring proper separation of**
1187 **staphylococcal daughter cells.**

1188 Under normal conditions, CxaR regulates Sle1 levels by delivering its precursor to ClpXP for
1189 degradation, ensuring that cell splitting is triggered only after septum completion. In the absence of
1190 CxaR, ClpX and ClpP still form a proteolytic complex capable of degrading various proteins, but not
1191 Sle1, as its mode of delivery is missing. Consequently, Sle1 accumulates to high levels, causing
1192 hydrolysis of the incomplete septum and subsequent cell lysis.